

# The Hyperspherical Geometry of Community Detection: Modularity as a Distance

**Martijn Gösgens**

*Eindhoven University of Technology, Eindhoven, Netherlands*

RESEARCH@MARTIJNGOSGENS.NL

**Remco van der Hofstad**

*Eindhoven University of Technology, Eindhoven, Netherlands*

R.W.V.D.HOFSTAD@TUE.NL

**Nelly Litvak**

*University of Twente, Enschede, Netherlands*

N.LITVAK@UTWENTE.NL

*Eindhoven University of Technology, Eindhoven, Netherlands*

## Abstract

The Louvain algorithm is currently one of the most popular community detection methods. This algorithm finds communities by maximizing a quantity called *modularity*. In this work, we describe a metric space of clusterings, where clusterings are described by a binary vector indexed by the vertex-pairs. We extend this geometry to a hypersphere and prove that maximizing modularity is equivalent to minimizing the angular distance to some *modularity vector* over the set of clustering vectors. This equivalence allows us to view the Louvain algorithm as a nearest-neighbor search that approximately minimizes the distance to this modularity vector. By replacing this modularity vector by a different vector, many alternative community detection methods can be obtained. We explore this wider class and compare it to existing modularity-based methods. Our experiments show that these alternatives may outperform modularity-based methods. For example, when communities are large compared to vertex neighborhoods, a vector based on numbers of common neighbors outperforms existing community detection methods. While the focus of the present work is community detection in networks, the proposed methodology can be applied to any clustering problem where pair-wise similarity data is available.

## 1. Introduction

Complex networks often contain groups of nodes that are more connected internally than externally. In network science, such groups are often referred to as *communities*. Community detection is the task of detecting such groups in a network. There exist many variants of this task and many algorithms have been developed for them (Fortunato, 2010). In this work, we consider detecting non-overlapping communities, so that a community structure is represented by a partition of the network nodes into communities. We will refer to such partitions as *clusterings*. Note that this task is closely related to the more general field of clustering, as we are essentially clustering the network nodes based on network topology.

In the remainder of this section we explain the basic notations and key notions from the literature that we build upon in this work. We consider a simple undirected graph  $G$  with vertex-set  $[n] = \{1, \dots, n\}$ . For a vertex  $i \in [n]$ , we denote its degree by  $d_i^{(G)}$  and denote the total number of edges by  $m_G = \frac{1}{2} \sum_{i \in [n]} d_i^{(G)}$ . We will use the letters  $C$  and  $T$  to denote clusterings.

**Granularity.** The number of clusters that a clustering consists of will be denoted by  $|C|$ , while  $m_C$  denotes the number of intra-cluster vertex-pairs. The number of intra-cluster pairs is an integer between 0 (when  $|C| = n$ ) and the total number of vertex-pairs  $N = \binom{n}{2}$  (when  $|C| = 1$ ). The

extent to which a clustering resembles the first or latter of these extremes is often referred to as the *granularity* of a clustering: *fine-grained* clusterings consist of many small clusters while *coarse-grained* clusterings consist of a few large clusters. Granularity will be an important notion in this paper, and we will use the number of intra-cluster pairs  $m_C$  as a measure of the granularity. Alternatively, many other works simply quantify granularity by the number of clusters  $|C|$ , but the drawback is that it is insensitive to the sizes of the clusters. In other works (Romano et al., 2016; Vinh et al., 2009, 2010), Shannon entropy is used as a measure of granularity. A generalization of Shannon entropy has been shown to be related to  $m_C$  (Romano et al., 2016).

**Validation indices.** When the ground truth community structure is available, the performance of a community detection method can be evaluated by comparing the obtained candidate clustering to the ground truth. In order to do this, one needs to measure the similarity between the candidate and the true clustering. Functions that quantify this similarity are referred to as *validation indices*. There exist many different validation indices (Vinh et al., 2010; Lei et al., 2017) and which one is most suitable depends on the context of the application (Gösgens et al., 2019). In this work, we denote the ground truth clustering by  $T$  while we denote other (candidate) clusterings by  $C$ .

One popular class of validation indices are the *pair-counting functions*. Given clusterings  $T$  and  $C$ , these indices can be expressed as functions of the following four variables: the number of intra-cluster pairs  $m_T, m_C$  of  $T$  and  $C$ , respectively, the number of vertex-pairs  $m_{TC}$  that are intra-cluster pairs of both  $T$  and  $C$ , and the total number of vertex-pairs  $N$ . Examples of such pair-counting indices are the Rand index (Rand, 1971), the Jaccard index (Jaccard, 1912), the Hubert Index (Hubert, 1977) and the Correlation Coefficient (Gösgens et al., 2019). Many of these indices are known to have a bias towards either clusterings of fine or coarse granularity (Albatineh et al., 2006; Romano et al., 2016; Gösgens et al., 2019; Lei et al., 2017). The Jaccard index is known to be biased towards coarse-grained clusterings while the bias of Rand depends on the granularity of the ground truth (Lei et al., 2017). The Correlation Coefficient does not suffer from such bias and additionally satisfies many other desirable properties (Gösgens et al., 2019). This correlation coefficient is given by

$$CC(T, C) = \frac{m_{TC}N - m_T m_C}{\sqrt{m_T \cdot (N - m_T) \cdot m_C \cdot (N - m_C)}}. \quad (1)$$

One of the desirable properties of the correlation coefficient that we will make grateful use of is that it can be transformed to a metric distance by taking its arccosine (Gösgens et al., 2019). This *Correlation Distance* plays a central role in this work and will be used as the main validation index throughout this paper.

**Modularity.** One of the most popular ways to detect communities is by maximizing a quantity called *modularity* (Newman and Girvan, 2004; Reichardt and Bornholdt, 2006). Modularity is based on the paradigm that a graph with community structure has many more intra-communities edges than it would have if one were to rewired the edges at random.

Given a clustering  $C$  and a graph  $G$ , modularity measures the difference between the number of intra-cluster edges that are present in  $G$  and the expected number of intra-cluster edges if  $G$  were to be rewired according to some random graph model without community structure. Such a random graph model is usually referred to as a *null model*. While it is theoretically possible to use any random graph model as a null model, the only null models that are commonly used in the literature are the Erdős-Rényi (ER) model and Configuration Model (CM).

**The resolution limit.** In large graphs, modularity maximization is known to be unable to detect communities below a given size. This *resolution limit* (Fortunato and Barthélemy, 2007; Kumpula

et al., 2007; Lancichinetti and Fortunato, 2011) is a large drawback of modularity-based methods. Basically, this means that modularity maximization is implicitly tuned to detect clusterings of a certain granularity. Modularity is often extended to include a *resolution parameter* to alleviate this problem (Reichardt and Bornholdt, 2006; Kumpula et al., 2007). However, this resolution parameter merely allows one to tune the detection method to a different granularity (Arenas et al., 2008), and does not address the fundamental problem that modularity implicitly has a bias towards clusterings of some granularity (Kumpula et al., 2007; Traag et al., 2011). Furthermore, it is nontrivial to find a resolution parameter value so that modularity optimization is tuned to the desired granularity in a given setting (Arenas et al., 2008; Prokhorenkova, 2019). Recently, modularity optimization has been shown to be equivalent to likelihood maximization (Newman, 2016): for a particular value of the resolution parameter, ER-modularity is equivalent to the likelihood function of a Planted Partition Model while CM-modularity is equivalent to the likelihood of a Degree-Corrected Stochastic Block Model. While this provides a mathematically principled approach to choosing the resolution parameter (Prokhorenkova and Tikhonov, 2019), it does require making assumptions about the distribution that the network was drawn from and knowledge of its parameters.

**The Louvain algorithm.** Despite its shortcomings, modularity maximization remains one of the most popular approaches for community detection. In applications, an additional difficulty arises from the fact that modularity maximization is NP-hard Brandes et al. (2007), which makes its exact maximization infeasible for large graphs. Therefore, practitioners often resort to *approximate* optimization algorithms. The most popular modularity-optimization is the so-called Louvain algorithm (Blondel et al., 2008), which is known to find an approximate modularity maximum in roughly log-linear time. The Louvain algorithm is also known to efficiently optimize other partition-based functions (Prokhorenkova and Tikhonov, 2019). Recently, some improvements to the Louvain algorithm have been made, resulting in algorithms of similar running time that reach better maxima (Traag et al., 2019). However, these improved algorithms are generally not as easily extended to other partition-based functions. For this reason, we limit ourselves to the Louvain algorithm for the remainder of the paper.

In the next section we will outline our methodology and provide an overview of the paper.

## 2. Outline of the methodology

The central idea of this paper is to describe a *hypersphere geometry* on the set of clusterings. In terms of this geometry, we prove that maximizing modularity is equivalent to minimizing the angular distance to some point that we call the *modularity vector*, over the set of clusterings. Replacing this modularity vector with a different vector leads to extensions of modularity-based methods. We thus obtain the following general class of community detection methods, containing all modularity-based methods, as well as other methods:

- Given a graph  $G$ , we map it to an appropriate *query vector*  $\mathbf{q}(G)$  in our hypersphere geometry. This query vector is indexed by vertex pairs. Such a query vector could be based on edge presences, as for ER-modularity, or involve the vertex-degrees, as for CM-modularity, but there are many other possibilities, such as the number of common neighbors between the pair of vertices.
- We then find a clustering by minimizing the distance to this query vector. Let  $\mathcal{C}(\mathbf{q}(G))$  denote the clustering vector that minimizes the distance to  $\mathbf{q}(G)$  over the set of all clusterings. Because it is computationally infeasible to *exactly* minimize this distance, we use the popular Louvain algorithm  $\mathcal{L}$  to find a clustering that *approximately* minimizes this distance. Hence,

our community detection method can be denoted by  $\mathcal{L}(\mathbf{q}(G))$ , which is an approximation of the solution to the minimization problem, obtained using the Louvain method.

In this setup, the way we map a graph to a query vector determines what clusterings are ‘near’ the graph. Hence, this *query mapping* largely determines how we detect communities. Given any vector  $\mathbf{x}$  that is derived from the graph  $G$ , we will provide a geometrically-inspired method to obtain a suitable query vector  $\mathbf{q}^*(\mathbf{x})$  from it. If this vector  $\mathbf{x}$  is simply a binary vector representing the edge-connectivity of a network, then the resulting community detection method is equivalent to maximizing ER-modularity for a particular value of the resolution parameter. Thus, our geometrical framework prescribes a value for the resolution parameter of ER-modularity. We compare this resolution parameter to the resolution parameter derived from likelihood-based methods. Our experiments indicate that our method performs on par (in terms of validation scores), but results in candidate clusterings that match the true granularity more closely than these likelihood-based methods. Similarly, when applying our geometric method to the CM-modularity vector, we obtain a detection method that also works on par with likelihood-based methods while matching the granularity more closely.

When applying this geometric method to vectors other than the binary edge-connectivity vector, we obtain community detection methods that do not necessarily correspond to maximizing modularity, or other existing community detection methods. For example, one can construct a vector where each entry corresponds to the number of common neighbors between each vertex pair. Our experiments indicate that the community detection method that results from this outperforms existing modularity-based methods whenever communities are large compared to vertex-neighborhoods.

While the focus of the present paper is community detection in networks, the proposed method is not limited to networks alone and is able to cluster *any* pair-wise similarity data. Suppose one has a vector  $\mathbf{x}$  indexed by the vertex-pairs such that  $\mathbf{x}_{ij}$  tends to be high when elements  $i$  and  $j$  are similar and low when they are unrelated. Then our method prescribes how to transform this vector to a query vector  $\mathbf{q}^*(\mathbf{x})$  such that a candidate clustering can be obtained by computing  $\mathcal{L}(\mathbf{q}^*(\mathbf{x}))$  by the Louvain algorithm.

**Organisation of this paper.** This paper is organised as follows. In Section 3, we describe the hypersphere geometry on the set of clusters. In Section 4, we show that maximizing modularity is equivalent to minimizing the angular distance to a modularity vector. In Section 5, we introduce an alternative query mapping to illustrate that this geometric viewpoint allows for extensions beyond modularity-based methods. In Section 6, we describe how a query vector can be ‘tuned’ to result in a candidate clustering with a desired level of granularity. The proposed community detection methods are experimentally compared to existing modularity-based methods in Section 7.

### 3. The hyperspherical geometry of clustering

For a given clustering  $C$ , we define  $\mathbf{b}(C)$  as the binary  $N$ -dimensional vector indexed by the vertex-pairs, where  $\mathbf{b}(C)_{ij}$  equals  $+1$  if  $i$  and  $j$  are assigned the same cluster in  $C$  and  $-1$  otherwise. In this work, binary vectors will have entries  $+1$  and  $-1$  unless specified otherwise. In particular cases, binary vectors with values  $1$  and  $0$  will be more convenient, we will refer to these as  $\{0, 1\}$ -binary vectors in contrast to  $\pm 1$  binary vectors. Note that not all  $\pm 1$  binary vectors correspond to clusterings, since the vector needs to satisfy transitivity. That is, for vertices  $i, j, k$ , it must hold that if  $\mathbf{b}(C)_{ij} = \mathbf{b}(C)_{jk} = 1$  then  $\mathbf{b}(C)_{ik} = 1$ . Furthermore, every binary vector that does satisfy this transitivity condition corresponds to precisely one clustering  $C$ . Importantly, note that all binary vectors have equal (Euclidean) length  $\sqrt{N}$ , hence, all clustering vectors lie on a hypersphere with radius  $\sqrt{N}$  centered around the origin.

For clusterings  $C_1, C_2$ , the *angular distance* between their binary vectors is given by

$$d_a(\mathbf{b}(C_1), \mathbf{b}(C_2)) = \arccos \left( \frac{\langle \mathbf{b}(C_1), \mathbf{b}(C_2) \rangle}{N} \right). \quad (2)$$

We can easily extend this metric space to the full hypersphere to allow for non-binary vectors. For  $\mathbf{x}, \mathbf{y} \in \mathbb{R}^N$  the angular distance is

$$d_a(\mathbf{x}, \mathbf{y}) = \arccos \left( \frac{\langle \mathbf{x}, \mathbf{y} \rangle}{\|\mathbf{x}\| \cdot \|\mathbf{y}\|} \right).$$

Furthermore, the correlation distance, which is defined as the arccosine of the correlation coefficient as given in (1), can similarly be extended to the full hypersphere by

$$d_{CC}(\mathbf{x}, \mathbf{y}) = \arccos \left( \frac{\langle \mathbf{x}, \mathbf{y} \rangle - \frac{\langle \mathbf{x}, \mathbf{1} \rangle \langle \mathbf{y}, \mathbf{1} \rangle}{N}}{\sqrt{\|\mathbf{x}\|^2 - \frac{\langle \mathbf{x}, \mathbf{1} \rangle^2}{N}} \sqrt{\|\mathbf{y}\|^2 - \frac{\langle \mathbf{y}, \mathbf{1} \rangle^2}{N}}} \right). \quad (3)$$

We note that the length of a vector has no meaning in these metric spaces. That is, scaling a vector by a positive scalar does not affect the (angular or correlation) distance to any other vector. This introduces an equivalence relation among vectors, where each equivalence class corresponds to a direction, the representative element of each of these classes will be the vector that is on the surface of the hypersphere, given by the *hypersphere projection*

$$\mathcal{H}(\mathbf{x}) = \frac{\sqrt{N}}{\|\mathbf{x}\|} \mathbf{x}.$$

All the definitions in the remainder of this section are invariant under this hypersphere projection.

**Hyperspherical geometry.** The angular distance defines a geometry on our hypersphere. We now introduce some basic hyperspherical geometry theory that will be needed later on. These hyperspherical results are direct analogues of their spherical counterparts. We refer to Todhunter (1863) and Donnay (2011) for a more complete overview of spherical geometry and trigonometry.

For any two-dimensional plane that contains the origin, its intersection with the hypersphere corresponds to a *great circle* (e.g., the equator of a globe), which is the closest hyperspherical analogue to an infinite straight line in Euclidean geometry. Therefore, we will refer to segments of a great circle as *hyperspherical straight lines*. The length of a hyperspherical straight line between two points corresponds to the angular distance between its endpoints. The definition of a hyperspherical angle (the angle that two hyperspherical straight lines make on the hypersphere) is less straightforward: given three distinct points  $\mathbf{x}, \mathbf{y}, \mathbf{z}$  on the hypersphere, the hyperspherical angle  $\angle(\mathbf{x}, \mathbf{y}, \mathbf{z})$  that the line from  $\mathbf{x}$  to  $\mathbf{y}$  makes with the line from  $\mathbf{z}$  to  $\mathbf{y}$  at  $\mathbf{y}$  is given by the *hyperspherical cosine rule*:

$$\cos \angle(\mathbf{x}, \mathbf{y}, \mathbf{z}) = \frac{\cos d_a(\mathbf{x}, \mathbf{z}) - \cos d_a(\mathbf{x}, \mathbf{y}) \cos d_a(\mathbf{y}, \mathbf{z})}{\sin d_a(\mathbf{x}, \mathbf{y}) \sin d_a(\mathbf{y}, \mathbf{z})}. \quad (4)$$

This angle is obtained by projecting  $\mathbf{x}$  and  $\mathbf{z}$  on the tangent plane of  $\mathbf{y}$  on the hypersphere and then simply computing the angle for these projected points via the (Euclidean) cosine rule, as illustrated in Figure 1. Similarly, for a hyperspherical triangle, the *hyperspherical sine rule* is given by

$$\frac{\sin \angle(\mathbf{x}, \mathbf{y}, \mathbf{z})}{\sin d_a(\mathbf{x}, \mathbf{z})} = \frac{\sin \angle(\mathbf{y}, \mathbf{x}, \mathbf{z})}{\sin d_a(\mathbf{y}, \mathbf{z})} = \frac{\sin \angle(\mathbf{x}, \mathbf{z}, \mathbf{y})}{\sin d_a(\mathbf{x}, \mathbf{y})}. \quad (5)$$

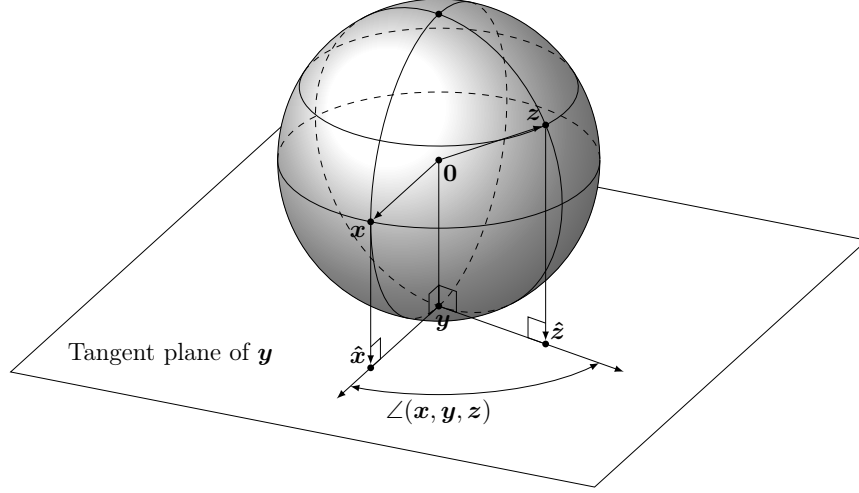


Figure 1: Illustration of the hyperspherical angle  $\angle(\mathbf{x}, \mathbf{y}, \mathbf{z})$  in the three-dimensional subspace spanned by  $\mathbf{x}, \mathbf{y}, \mathbf{z}$ . The solid arcs are on the visible side of the sphere while the dashed arcs are on the back side. The vectors  $\hat{\mathbf{x}}$  and  $\hat{\mathbf{z}}$  are the projections of  $\mathbf{x}, \mathbf{z}$  respectively to the tangent plane of  $\mathbf{y}$ . For  $\mathbf{y} = -\mathbf{1}$ , we have  $\angle(\mathbf{x}, -\mathbf{1}, \mathbf{z}) = d_{CC}(\mathbf{x}, \mathbf{z})$ .

If one of the hyperspherical angles in a triangle is a right angle, say  $\angle(\mathbf{x}, \mathbf{y}, \mathbf{z}) = \pi/2$ , then the hyperspherical cosine rule can be rewritten to the *hyperspherical Pythagorean theorem*, given by

$$\cos d_a(\mathbf{x}, \mathbf{z}) = \cos d_a(\mathbf{x}, \mathbf{y}) \cos(\mathbf{y}, \mathbf{z}). \quad (6)$$

In addition, we get the right-angle formulae, stating that, when  $\angle(\mathbf{x}, \mathbf{y}, \mathbf{z}) = \pi/2$ ,

$$\sin \angle(\mathbf{y}, \mathbf{x}, \mathbf{z}) = \frac{\sin d_a(\mathbf{y}, \mathbf{z})}{\sin d_a(\mathbf{x}, \mathbf{z})}, \quad \text{and} \quad \cos \angle(\mathbf{y}, \mathbf{x}, \mathbf{z}) = \frac{\tan d_a(\mathbf{x}, \mathbf{y})}{\tan d_a(\mathbf{x}, \mathbf{z})}. \quad (7)$$

These elementary results are needed for several proofs in Section 6.

**Poles.** In the metric space described previously, the all-one vector  $\mathbf{1}$  corresponds to the clustering where all items are put in the same cluster, while the vector  $-\mathbf{1}$  corresponds to the clustering where each item is placed in its own separate cluster. These two points form opposite *poles* on our hypersphere. Clusterings lying close to  $\mathbf{1}$  correspond to clusterings of coarse granularity (i.e., consisting of relatively few and large clusters), while clusters close to  $-\mathbf{1}$  correspond to clusterings of fine granularity. Therefore, we will refer to  $\mathbf{1}$  as the *coarse pole* while we will refer to  $-\mathbf{1}$  as the *fine pole*.

**Latitudes.** In analogy to the terminology used for globes, we refer to the angular distance to the fine pole as the *latitude* of a point. The difference is that in geography, latitude is usually defined as the angular distance to the equator, while we take the angular distance to the (fine) pole. We thus define the latitude of a vector  $\mathbf{x}$  by

$$\ell(\mathbf{x}) = d_a(\mathbf{x}, -\mathbf{1}) = \arccos \left( \frac{-\langle \mathbf{x}, \mathbf{1} \rangle}{\sqrt{N} \cdot \|\mathbf{x}\|} \right). \quad (8)$$

For a clustering  $C$ , (8) depends only on the number of intra-cluster pairs (or, equivalently, the the number of +1's in  $\mathbf{b}(C)$ ), which we denote by  $m_C$ :

$$\ell(\mathbf{b}(C)) = \arccos \left( \frac{-m_C + (N - m_C)}{\sqrt{N} \cdot \sqrt{N}} \right) = \arccos \left( 1 - \frac{2m_C}{N} \right). \quad (9)$$

We refer to the *equator* as the set of points at equal distance to both poles, that is, with latitude  $\pi/2$ , or equivalently, the set of vectors  $\mathbf{x}$  with  $\langle \mathbf{x}, \mathbf{1} \rangle = 0$ . This contains the clustering vectors for clusterings that have an equal number of inter- and intra-cluster pairs. From (9) we see that  $\ell(\mathbf{b}(C)) > \pi/2$  occurs only when  $C$  has more intra-cluster pairs than inter-cluster pairs. Moreover, it can be shown that any clustering with  $\ell(\mathbf{b}(C)) > \pi/2$  has a cluster of size larger than  $n/2$ , which is usually not the case when clustering into more than two clusters. This tells us that clusterings generally lie on the fine hemisphere. Furthermore, let  $n \rightarrow \infty$  and suppose the expected community size of a randomly chosen vertex is  $s$  and does not depend on  $n$ , then the latitude of a ground truth community structure shrinks like

$$\arccos(1 - 2\frac{s-1}{n-1}) = 2\sqrt{\frac{s-1}{n-1}} + o(n^{-1}), \quad (10)$$

so that for large  $n$ , clusterings are concentrated around the fine pole.

**Meridians and parallels.** In the same geographic analogy, a *meridian* is a hyperspherical straight line between the poles, while a *parallel* is a hypersurface of constant latitude. Note, however, that in the three-dimensional real-world, a parallel is a one-dimensional object while in our case it has dimension  $N - 2$ .

For every vector  $\mathbf{x}$  that is not a multiple of  $\mathbf{1}$ , there is precisely one meridian running through its hypersphere projection. Similarly, every vector  $\mathbf{x}$  lies on exactly one parallel, namely the parallel with latitude  $\ell(\mathbf{x})$ . Therefore, each point on the hypersphere is uniquely defined by a meridian and a latitude. The point that lies on the meridian of  $\mathbf{x}$  and has latitude  $\lambda$  is equal to the projection of  $\mathbf{x}$  onto the parallel with latitude  $\lambda$ . This *parallel projection* is given by

$$\mathcal{P}_\lambda(\mathbf{x}) = \sin(\lambda)\mathcal{H}\left(\mathbf{x} - \frac{\langle \mathbf{x}, \mathbf{1} \rangle}{N}\mathbf{1}\right) - \cos(\lambda)\mathbf{1}. \quad (11)$$

Since the equator corresponds to the parallel with latitude  $\pi/2$ , the projection to the equator is given by  $\mathcal{P}_{\pi/2}(\mathbf{x})$ .

All meridians meet at both poles. Given two meridians that run through  $\mathbf{x}$  and  $\mathbf{y}$  respectively, we can compute the hyperspherical angle that they make at the fine pole. We will refer to this as the *meridian angle* between  $\mathbf{x}$  and  $\mathbf{y}$ . For  $\mathbf{x}, \mathbf{y}$  with latitudes in  $(0, \pi)$ , the meridian angle can be computed via the hyperspherical cosine rule (4) and is given by

$$\text{MeridianAngle}(\mathbf{x}, \mathbf{y}) = \angle(\mathbf{x}, -\mathbf{1}, \mathbf{y}) = \arccos\left(\frac{\cos d_a(\mathbf{x}, \mathbf{y}) - \cos \ell(\mathbf{x}) \cos \ell(\mathbf{y})}{\sin \ell(\mathbf{x}) \sin \ell(\mathbf{y})}\right). \quad (12)$$

Alternatively, this meridian angle can be written as  $d_a(\mathcal{P}_{\pi/2}(\mathbf{x}), \mathcal{P}_{\pi/2}(\mathbf{y}))$ . By convention, we define this angle to be zero when both vectors are on the same pole,  $\pi$  when both vectors are on opposite poles and  $\pi/2$  when one vector is on a pole while the other is not. We prove the following result:

**Theorem 1** *For all  $\mathbf{x}, \mathbf{y} \in \mathbb{R}^N$ ,  $\text{MeridianAngle}(\mathbf{x}, \mathbf{y}) = d_{\text{CC}}(\mathbf{x}, \mathbf{y})$  holds. That is, the meridian angle coincides with the correlation distance.*

**Proof** We will prove the theorem by showing that the cosine of the meridian angle in (12) and the cosine of the correlation distance (3) are the same. From (12) we directly get

$$\cos(\text{MeridianAngle}(\mathbf{x}, \mathbf{y})) = \frac{\cos d_a(\mathbf{x}, \mathbf{y}) - \cos \ell(\mathbf{x}) \cdot \cos \ell(\mathbf{y})}{\sqrt{1 - \cos^2 \ell(\mathbf{x})} \cdot \sqrt{1 - \cos^2 \ell(\mathbf{y})}}.$$

Next, we multiply both numerator and denominator by  $\|\mathbf{x}\| \cdot \|\mathbf{y}\|$  to obtain

$$\frac{\|\mathbf{x}\| \cdot \|\mathbf{y}\| \cos d_a(\mathbf{x}, \mathbf{y}) - \|\mathbf{x}\| \cos \ell(\mathbf{x}) \cdot \|\mathbf{y}\| \cos \ell(\mathbf{y})}{\sqrt{\|\mathbf{x}\|^2 - (\|\mathbf{x}\| \cos \ell(\mathbf{x}))^2} \cdot \sqrt{\|\mathbf{y}\|^2 - (\|\mathbf{y}\| \cos \ell(\mathbf{y}))^2}}.$$

After substituting  $\|\mathbf{x}\| \cdot \|\mathbf{y}\| \cos d_a(\mathbf{x}, \mathbf{y}) = \langle \mathbf{x}, \mathbf{y} \rangle$ ,  $\|\mathbf{x}\| \cos \ell(\mathbf{x}) = -\langle \mathbf{x}, \mathbf{1} \rangle / \sqrt{N}$  (see (8)) and similarly  $\|\mathbf{y}\| \cos \ell(\mathbf{y}) = -\langle \mathbf{y}, \mathbf{1} \rangle / \sqrt{N}$ , the resulting expression is the same as the argument of the arccosine in the right-hand side of (3).

We next check the boundary cases, where  $\mathbf{x}$  or  $\mathbf{y}$  are poles: The case where both  $\mathbf{x}$  and  $\mathbf{y}$  are on the same pole corresponds to comparing two constant vectors of the same sign, which gives correlation 1 and thus results in a correlation distance of 0, which is equal to the meridian angle by our definition. Similarly, when both vectors are on different poles, then they are constant vectors of different signs, hence, the correlation coefficient is  $-1$ , and the correlation distance again equals the meridian angle  $\pi$ . Finally, when one vector is on the pole and the other is not, then (3) gives  $d_{CC}(\mathbf{x}, \mathbf{y}) = \pi/2$ , again in accordance with our definition of the meridian angle. ■

Theorem 1 provides a new interpretation for the correlation distance. Furthermore, since the correlation distance defines a distance on the set of clustering vectors, it can be zero only when clusterings are equal. This implies that, surprisingly, all clustering vectors, except the poles, lie on different meridians. To avoid using two different notations for the same quantity, we will denote the meridian angle by  $d_{CC}$  in the remainder of this paper.

**Pair-counting distance metrics.** The correlation distance is not the only pair-counting validation index that is related to this hyperspherical geometry: the cosine of the angular distance  $d_a$  is equal to the Hubert index (Hubert, 1977). This Hubert index is related to the Rand index by  $\text{Hubert}(C_1, C_2) = 2\text{Rand}(C_1, C_2) - 1$  while the Rand index is related to the Euclidean distance  $d_E$  by

$$\text{Rand}(C_1, C_2) = 1 - \frac{d_E(\mathbf{b}(C_1), \mathbf{b}(C_2))^2}{4N}.$$

These two relations are relevant because modularity can be related to both Euclidean and angular distance, as will be proven in Section 4.

#### 4. Modularity as a distance

In the previous section, we have shown how clusterings can be mapped to the vector space  $\mathbb{R}^N$  in a meaningful way by the mapping  $\mathbf{b}(\cdot)$ . In the present section, we discuss how graphs can be mapped to the vector space in a similar way. This is the next step in our methodology that formalizes community detection methods as algorithms that find a candidate community structure  $C$  by minimizing the distance between its binary vector  $\mathbf{b}(C)$  and the *query vector*  $\mathbf{q}(G)$  that the graph is mapped to. Here, the function  $\mathbf{q}(\cdot)$  maps graphs of size  $n$  to vectors in  $\mathbb{R}^N$ , and will be referred to as a *query mapping*. Such a mapping can be made in many different ways and we will discuss a few interesting options.

**Query vectors versus affinity matrices.** When executing community detection, we want to find  $\mathbf{q}(G)$  such that the nearest clustering vector is close to the ‘true’ clustering  $T$ . Therefore, ideally,  $\mathbf{q}(G)$  should be chosen in such a way that  $\mathbf{b}(T)$  is one of its closest clustering vectors. To achieve this, we wish  $\mathbf{q}(G)_{ij}$  to be positive whenever  $ij$  is an intra-community pair of  $T$  and negative otherwise. In that sense, query vectors are related to the notion of an *affinity matrix* that is used throughout the clustering literature (Xu and Wunsch, 2005; Filippone et al., 2008), where the

pairwise similarities are summarized by an  $n \times n$  symmetric matrix. Existing clustering algorithms use this matrix in various ways to cluster the elements. For example, the popular Spectral Clustering algorithm computes the leading eigenvectors of the affinity matrix and then clusters the items based on these vectors (Filippone et al., 2008). In our context, the  $\binom{n}{2} = N$  entries of a pair-wise vector correspond to the entries of the upper (or lower) triangle of this affinity matrix. While for many operations, such as computing eigenvectors, a matrix representation of similarity is natural, we find that in our geometric setting a vector representation is more appropriate because we heavily rely on inner products.

The simplest way to map a graph  $G$  to a vector is by a binary *edge-connectivity vector*  $\mathbf{e}(G)$ , where  $\mathbf{e}(G)_{ij}$  equals +1 if vertices  $i$  and  $j$  are connected by an edge and  $-1$  otherwise. We note that this mapping  $\mathbf{e}(\cdot)$  forms a bijection between the set of simple undirected graphs of  $n$  vertices and the set of binary vectors. However, there are many more ways in which a graph can be mapped to  $\mathbb{R}^N$ . In Theorem 2 below we show that maximizing modularity  $M_\gamma(C, G; \mathcal{N})$  for any null-model  $\mathcal{N}$  and resolution parameter  $\gamma$ , is equivalent to minimizing the distance between the clustering vector  $\mathbf{b}(C)$  and the *modularity vector*  $\mathbf{q}(G) = \mathbf{q}_M(G; \mathcal{N}, \gamma)$ . Let the  $N$ -dimensional vector  $\mathbf{p}(G; \mathcal{N})$  denote the expected number of edges that each vertex-pair of  $G$  has when the edges are rewired according to a null-model  $\mathcal{N}$ . This vector is non-negative and its entries sum to the total number of edges  $m_G$  as, in total, no edges are removed or added. For an Erdős-Rényi null model and the configuration model<sup>1</sup>, these vectors are respectively given by

$$\mathbf{p}(G; \text{ER}) = \frac{m_G}{N} \mathbf{1}, \quad \text{and} \quad \mathbf{p}(G; \text{CM})_{ij} = \frac{d_i^{(G)} d_j^{(G)}}{2m_G}. \quad (13)$$

Then we define the modularity vector with respect to null model  $\mathcal{N}$  and resolution parameter  $\gamma$  as

$$\mathbf{q}_M(G; \mathcal{N}, \gamma) = \mathbf{1} + \mathbf{e}(G) - 2\gamma \mathbf{p}(G; \mathcal{N}). \quad (14)$$

We now present the main result of this section:

**Theorem 2** *For a null model  $\mathcal{N}$  and resolution parameter  $\gamma$ , maximizing modularity  $M_\gamma(C, G; \mathcal{N})$  over all clusterings  $C$  is equivalent to minimizing either*

- (i) *the Euclidean distance  $d_E(\mathbf{b}(C), \mathbf{q}_M(G; \mathcal{N}, \gamma))$  over all clusterings  $C$ ; or*
- (ii) *the angular distance  $d_a(\mathbf{b}(C), \mathbf{q}_M(G; \mathcal{N}, \gamma))$  over all clusterings  $C$ .*

Theorem 2 thus gives a geometric interpretation of modularity maximization. We will see that this geometric interpretation is useful. For example, it allows for various extensions and provides a new interpretation for the resolution parameter  $\gamma$ , as we explain in more detail below. To prove Theorem 2, we first need to prove the following lemma:

**Lemma 3** *Minimizing the Euclidean distance to some  $\mathbf{v}$  over the set of  $\pm 1$  binary vectors  $\mathbf{b}$  is equivalent to minimizing the angular distance between  $\mathbf{b}$  and  $\mathbf{v}$ .*

**Proof** The result follows after we relate the square of the Euclidean distance to the cosine of the angular distance, and then use the fact that any binary vector  $\mathbf{b}$  has length  $\sqrt{N}$ :

$$\begin{aligned} d_E(\mathbf{b}, \mathbf{v})^2 &= \|\mathbf{b}\|^2 + \|\mathbf{v}\|^2 - 2\langle \mathbf{b}, \mathbf{v} \rangle \\ &= N + \|\mathbf{v}\|^2 - 2\|\mathbf{v}\|\sqrt{N} \cos d_a(\mathbf{b}, \mathbf{v}). \end{aligned}$$

---

1. Actually, the denominator should be  $2m_G - 1$  but this is usually simplified to  $2m_G$ .

Now  $N$  and  $\|\mathbf{v}\|$  are constant w.r.t.  $\mathbf{b}$  and can thus be ignored. This tells us that minimizing the Euclidean distance is equivalent to maximizing the cosine of the angular distance, or equivalently, minimizing the angular distance. This completes the proof. ■

We are now ready to prove Theorem 2:

**Proof of Theorem 2** Modularity can be written as

$$M_\gamma(C, G; \mathcal{N}) = \frac{1}{m_G} \langle \frac{1}{2}(\mathbf{1} + \mathbf{b}(C)), \frac{1}{2}(\mathbf{1} + \mathbf{e}(G)) - \gamma \mathbf{p}(G; \mathcal{N}) \rangle. \quad (15)$$

We multiply this with  $4m_G$  and subtract  $\langle \mathbf{1}, \mathbf{1} + \mathbf{e}(G) - 2\gamma \mathbf{p}(G; \mathcal{N}) \rangle$ , which are both constant w.r.t.  $C$ . This yields

$$\langle \mathbf{b}(C), \mathbf{1} + \mathbf{e}(G) - 2\gamma \mathbf{p}(G; \mathcal{N}) \rangle = \|\mathbf{b}(C)\| \cdot \|\mathbf{q}_M(G; \mathcal{N}, \gamma)\| \cos d_a(\mathbf{b}(C), \mathbf{q}_M(G; \mathcal{N}, \gamma)).$$

Finally,  $\|\mathbf{b}(C)\| = \sqrt{N}$  and  $\|\mathbf{q}_M(G; \mathcal{N}, \gamma)\|$  are constant w.r.t.  $C$ . From this, we conclude that maximizing modularity is equivalent to maximizing the cosine of the angular distance. Since the arccosine is a strictly decreasing function on  $[-1, 1]$ , it follows that maximizing modularity is equivalent to minimizing the angular distance. The equivalence to the Euclidean distance follows from Lemma 3. ■

Theorem 2 relates modularity to a hyperspherical geometry as well as a Euclidean geometry, while the latter has one more dimension than the former. This can be explained by the fact that rescaling the query vector does not affect the optimization, as shown in Lemma 3. Therefore, the length of a query vector in Euclidean space has no effect on the resulting candidate clustering. Therefore, we focus on the hyperspherical geometry for the remainder of this work.

**Louvain as an approximate nearest-neighbor search.** Let us denote a clustering vector that minimizes the angular distance to the query vector  $\mathbf{q}$  by  $\mathcal{C}(\mathbf{q})$ . Possibly, there are multiple clustering vectors at minimal distance to the query vector. In such cases, we choose  $\mathcal{C}(\mathbf{q})$  arbitrarily (but deterministically) out of them.

Note that  $\mathcal{C}(\mathbf{q})$  is a *nearest neighbor* of the query vector  $\mathbf{q}$  among the clustering vectors. However, from Theorem 2 it follows that finding  $\mathcal{C}(\mathbf{q}_M(G; \mathcal{N}, \gamma))$  is equivalent to finding the global modularity maximum, which is known to be NP-hard (Brandes et al., 2007). Therefore, most modularity-maximizing algorithms, such as the popular Louvain algorithm (Blondel et al., 2008), *approximately* maximize modularity, resulting in an *approximate nearest neighbor* of the modularity vector. Hence, the Louvain algorithm can be viewed as an *approximate nearest neighbor search*.

While the Louvain algorithm was initially introduced for CM-modularity-maximization, it is known to be able to efficiently optimize other clustering-functions as well (Traag et al., 2011; Prokhorenkova and Tikhonov, 2019). In this work, we use the Louvain algorithm to minimize the angular distance to a query vector. Let  $\mathcal{L}(\mathbf{q})$  denote the approximate nearest neighbor obtained by applying the Louvain algorithm to a query vector  $\mathbf{q}$ . Because  $\mathcal{L}(\mathbf{q})$  is an approximate nearest neighbor of  $\mathbf{q}$ , we expect it to satisfy

$$d_a(\mathcal{L}(\mathbf{q}), \mathbf{q}) \approx d_a(\mathcal{C}(\mathbf{q}), \mathbf{q}),$$

though  $d_a(\mathcal{L}(\mathbf{q}), \mathbf{q}) \geq d_a(\mathcal{C}(\mathbf{q}), \mathbf{q})$  will always hold as  $\mathcal{C}(\mathbf{q})$  is a global minimizer.

Furthermore, because the Louvain algorithm is a greedy algorithm that is initialized at the clustering corresponding to the fine pole  $-\mathbf{1}$ ,  $\mathcal{L}(\mathbf{q})$  cannot be further from  $\mathbf{q}$  than  $-\mathbf{1}$ , i.e.  $d_a(\mathcal{L}(\mathbf{q}), \mathbf{q}) \leq$

$d_a(-\mathbf{1}, \mathbf{q}) = \ell(\mathbf{q})$ . Combining this, we get

$$d_a(\mathcal{L}(\mathbf{q}), \mathbf{q}) \in [d_a(\mathcal{C}(\mathbf{q}), \mathbf{q}), \ell(\mathbf{q})]. \quad (16)$$

A mapping  $\mathcal{A}$  is a *projection* if  $\mathcal{A}(\mathcal{A}(\mathbf{x})) = \mathcal{A}(\mathbf{x})$  holds for all  $\mathbf{x} \in \mathbb{R}^N$ . It can easily be seen that the hypersphere projection  $\mathcal{H}$  and the parallel projection  $\mathcal{P}_\lambda$  for any  $\lambda \in [0, \pi]$  are indeed projections. Also, it holds that  $\mathcal{C}$  is a projection onto the set of clustering vectors, as  $\mathcal{C}(\mathbf{b}(C)) = \mathbf{b}(C)$  holds for all clustering vectors. In Appendix A, we furthermore prove that the Louvain algorithm is also a projection. Therefore, the community detection methods that are discussed in this work follow a two-step approach where the graph is first mapped to the query vector and then projected to the set of clustering vectors.

**Resolution and latitude.** The resolution parameter in the modularity function is closely related to the latitude of the corresponding modularity vector, as described by the following lemma:

**Lemma 4** *The line  $(\mathcal{H}(\mathbf{q}_M(G; \mathcal{N}, \gamma)))_{\gamma \geq 0}$  is the (hyperspherically) straight line that starts from  $\mathcal{H}(\mathbf{1} + \mathbf{e}(G))$ , intersects the equator at  $\gamma = 1$  and ends in  $\mathcal{H}(-\mathbf{p}(G; \mathcal{N}))$ . The resolution parameter relates to the latitude as*

$$\ell(\mathbf{q}_M(G; \mathcal{N}, \gamma)) = \arccos \left( \frac{(\gamma - 1)m_G}{\sqrt{N} \cdot \sqrt{(1 - \gamma)m_G + \gamma^2 \|\mathbf{p}(G; \mathcal{N})\|^2 - \gamma \langle \mathbf{p}(G; \mathcal{N}), \mathbf{e}(G) \rangle}} \right). \quad (17)$$

**Proof** For  $\gamma = 0$ , the modularity vector is given by  $\mathbf{q}_M(G; \mathcal{N}, 0) = \mathbf{1} + \mathbf{e}(G)$ , corresponding to the starting point of the line. The endpoint is obtained by

$$\lim_{\gamma \rightarrow \infty} \mathcal{H}(\mathbf{q}_M(G; \mathcal{N}, \gamma)) = \lim_{\gamma \rightarrow \infty} \sqrt{N} \frac{\mathbf{1} + \mathbf{e}(G) - 2\gamma \mathbf{p}(G; \mathcal{N})}{\|\mathbf{1} + \mathbf{e}(G) - 2\gamma \mathbf{p}(G; \mathcal{N})\|} = -\sqrt{N} \frac{\mathbf{p}(G; \mathcal{N})}{\|\mathbf{p}(G; \mathcal{N})\|} = \mathcal{H}(-\mathbf{p}(G; \mathcal{N})).$$

To prove that the curve  $\gamma \mapsto \mathcal{H}(\mathbf{q}_M(G; \mathcal{N}, \gamma))$  is a hyperspherical straight line, we must show that it is a segment of a great circle. Note that the line  $(\mathbf{q}_M(G; \mathcal{N}, \gamma))_{\gamma \geq 0}$  is contained in the 2-dimensional plane that is defined by the three vectors  $\mathbf{q}_M(G; \mathcal{N}, 0)$ ,  $-\mathbf{p}(G; \mathcal{N})$  and the origin. The intersection between this plane and the hypersphere defines a great circle. Since the projection  $(\mathcal{H}(\mathbf{q}_M(G; \mathcal{N}, \gamma)))_{\gamma \geq 0}$  is contained in the same plane and lies on the hypersphere, it must be a subset of the same great circle. Therefore,  $(\mathcal{H}(\mathbf{q}_M(G; \mathcal{N}, \gamma)))_{\gamma \geq 0}$  is a segment of a great circle, so that it is a hyperspherical straight line by definition. Finally, (17) is obtained by substituting the modularity vector, given by (14), into the latitude  $\ell$ , as given by (8) and using  $\langle \mathbf{p}(G; \mathcal{N}), \mathbf{1} \rangle = m_G$ . ■

In Lemma 4, we restrict to  $\gamma \geq 0$ . While modularity could also be defined for negative resolution parameter values, the optimization of modularity for  $\gamma < 0$  will always lead to clustering all items in the same cluster (i.e., the coarse pole). Lemma 4 can easily be extended to take these negative resolution parameters to show that  $(\mathcal{H}(\mathbf{q}_M(G; \mathcal{N}, \gamma)))_{\gamma \in \mathbb{R}}$  corresponds to the unique hyperspherical straight line from  $\mathcal{H}(\mathbf{p}(G; \mathcal{N}))$  to  $\mathcal{H}(-\mathbf{p}(G; \mathcal{N}))$  that passes  $\mathcal{H}(\mathbf{1} + \mathbf{e}(G))$ .

For the ER null-model, Lemma 4 tells us that the line  $\mathcal{H}(\mathbf{q}_M(G; \text{ER}, \gamma))_{\gamma \geq 0}$  lies on a single meridian, ranging from  $\mathcal{H}(\mathbf{1} + \mathbf{e}(G))$  to  $-\mathbf{1}$ . The latitudes of vectors on this meridian is given by

$$\tan \ell(\mathbf{q}_M(G; \text{ER}, \gamma)) = \frac{\sqrt{\frac{N - m_G}{m_G}}}{\gamma - 1},$$

as is derived in Appendix A.

**The hypersphere interpretation of the resolution limit.** A limitation of modularity-maximizing based methods is the well-known *resolution limit* (Fortunato and Barthélemy, 2007). The easiest example to demonstrate this resolution limit is by a ring of cliques (Fortunato and Barthélemy, 2007): consider a graph  $G_{k,s}$  that is given by a ring of  $k$  cliques each consisting of  $s$  vertices and let each pair of neighboring cliques be connected by a single edge. Such a graph has a natural clustering  $T_{k,s}$  into its  $k$  cliques. It can be shown that for any  $s > 2$  and sufficiently high  $k$ , a clustering that merges two neighboring cliques has a higher modularity value, which is clearly undesirable. While this result was initially only given for the CM null model and  $\gamma = 1$ , it easily generalizes to other null models, resolution parameter values and graph designs (Fortunato and Barthélemy, 2007; Traag et al., 2011).

The general problem is that in large sparse graphs, the expected number of edges between small communities is so negligibly small that the existence of *any* edge between them will be enough to result in a modularity-increase for merging these communities. In our geometric framework, we will show that this resolution limit can be characterized as a discrepancy between the latitude of the query vector and the latitude of the ground truth clustering vector. The inverse triangle inequality allows us to bound the angular distance by

$$d_a(\mathbf{b}(T), \mathbf{q}_M(G; \mathcal{N}, \gamma)) \geq |d_a(-\mathbf{1}, \mathbf{q}_M(G; \mathcal{N}, \gamma)) - d_a(-\mathbf{1}, \mathbf{b}(T))| = |\ell(\mathbf{q}_M(G; \mathcal{N}, \gamma)) - \ell(\mathbf{b}(T))|.$$

Note that for  $\gamma = 1$ , the modularity vector has latitude  $\pi/2$  while the latitude of the ground truth clustering vector decreases roughly like  $n^{-1/2}$ , as shown in (10). Therefore,  $d_a(\mathbf{b}(T), \mathbf{q}_M(G; \mathcal{N}, 1)) \approx \pi/2$  for large graphs. This means that  $\mathbf{b}(T)$  and  $\mathbf{q}_M(G; \mathcal{N}, \gamma)$  are far from each other on the hypersphere. Since modularity maximization returns clustering  $C$  such that  $\mathbf{b}(C)$  is close to  $\mathbf{q}_M(G; \mathcal{N}, \gamma)$ , this results in clustering  $C$  being far away from the ground truth clustering  $T$ . This characterizes the resolution limit as a discrepancy between the latitudes of the modularity vector and ground truth clustering vector.

However, a different choice for the query vector could avoid such a resolution limit: for the particular example of the ring of cliques  $G_{k,s}$ , the simple query mapping  $\mathbf{q}(G) = \mathbf{e}(G)$  would have angular distance

$$d_a(\mathbf{b}(T), \mathbf{e}(G_{k,s})) = \arccos\left(1 - 2\frac{k}{N}\right) \approx 2\sqrt{k/\binom{k \cdot s}{2}} = O(k^{-1/2}),$$

for  $k \rightarrow \infty$ . Therefore, the query mapping  $\mathbf{e}$  overcomes the resolution limit and is a better query mapping than the modularity query mapping for this particular graph. We emphasize that the choice of the query vector should depend on characteristics of the graph and community structure: for more realistic networks with larger and less dense communities, the query mapping  $\mathbf{q}(G) = \mathbf{e}(G)$  will perform poorly as its latitude will be small compared to that of the ground truth clustering. We note that  $\mathbf{e}(G)$  does lie on the same meridian as the ER-modularity vector  $\mathbf{q}_M(G; \text{ER}, 1)$ , which suggests that adjusting the latitude of the query vector may be a fruitful approach. In Section 6, we provide a general approach for choosing such a latitude.

Lemma 4 tells us that the resolution parameter is related to the latitude of the modularity vector. Moreover, the latitude has the advantage that it is defined for any query and clustering vector, while the resolution parameter only tells us something about the query vector  $\mathbf{q}_M(G; \mathcal{N}, \gamma)$ . Therefore, we suggest to use the latitude of the query vector, rather than the resolution parameter, as the quantity that regulates the granularity of the candidate clustering. We further elaborate on this idea in the remainder of the paper.

## 5. Query mappings based on common neighbors

As shown in Section 4, modularity merely corresponds to a subclass of possible query mappings, which can be replaced by alternative query mappings, for example,  $\mathbf{e}(G)$  for the ring of cliques. In this section we explore another promising alternative to exemplify the general approach. In Section 7, we present experiments that compare its performance to existing modularity-based query mappings.

Similarly as we have mapped the edge-connectivity of a graph  $G$  to the edge-connectivity query vector  $\mathbf{e}(G)$  in Section 4, we can express the number of common neighbors between each pair of vertices in terms of a vector as well. We will denote this vector by  $\mathbf{w}(G)$  and will refer to it as the *wedge vector*, because the entry  $\mathbf{w}(G)_{ij}$  corresponds to the number of distinct *wedges* (paths of length 2) that have the vertices  $i$  and  $j$  as endpoints. Intuitively,  $\mathbf{w}(G)$  is closely related to the community structure of  $G$  because disconnected vertices  $i$  and  $j$  of the same community may have many common neighbors, which makes  $\mathbf{w}(G)_{ij}$  high as well, and thus  $\mathbf{b}(C)$  will tend to be closer to  $\mathbf{w}(G)$  when clustering  $C$  puts  $i$  and  $j$  in the same community. In the experiments of Section 7, we will see that when communities are relatively large compared to vertex-neighborhoods, we will indeed have  $d_{\text{CC}}(\mathbf{w}(G), \mathbf{b}(T)) < d_{\text{CC}}(\mathbf{e}(G), \mathbf{b}(T))$ .

To provide further motivation for the claim that this wedge-vector is of interest, we relate it to the global clustering coefficient of the graph:

**Lemma 5** *The global clustering coefficient of a graph  $G$  is given by*

$$\text{GlobalClustering}(G) = \frac{1}{2} \left( 1 - \frac{\cos d_a(\mathbf{e}(G), \mathbf{w}(G))}{\cos \ell(\mathbf{w}(G))} \right).$$

**Proof** The global clustering coefficient is given by the fraction of wedges that are closed. Since each triangle consists of three closed wedges, this coefficient is given by thrice the number of triangles divided by the number of wedges. If there is an edge between  $i$  and  $j$ , then this edge  $ij$  is part of  $\mathbf{w}(G)_{ij}$  many triangles. Summing  $\mathbf{w}(G)_{ij}$  over all edges would thus give thrice the number of triangles, as each triangle contains three edges. In vector notation, this is given by  $\langle \frac{1}{2}(\mathbf{e}(G) + \mathbf{1}), \mathbf{w}(G) \rangle$ , where  $(\mathbf{e}(G) + \mathbf{1})/2$  is the  $\{0, 1\}$ -binary vector edge-connectivity vector. The total number of wedges is given by  $\langle \mathbf{1}, \mathbf{w}(G) \rangle$ . Combined, this allows us to write the clustering coefficient as

$$\text{GlobalClustering}(G) = \frac{\langle \frac{1}{2}(\mathbf{e}(G) + \mathbf{1}), \mathbf{w}(G) \rangle}{\langle \mathbf{1}, \mathbf{w}(G) \rangle} = \frac{1}{2} \left( 1 + \frac{\langle \mathbf{e}(G), \mathbf{w}(G) \rangle}{\langle \mathbf{1}, \mathbf{w}(G) \rangle} \right).$$

Finally, from the definitions of the angular distance and latitude, as given by (2) and (8), it follows that

$$\frac{\langle \mathbf{e}(G), \mathbf{w}(G) \rangle}{\langle \mathbf{1}, \mathbf{w}(G) \rangle} = -\frac{\cos d_a(\mathbf{e}(G), \mathbf{w}(G))}{\cos \ell(\mathbf{w}(G))},$$

which completes the proof. ■

Since  $\cos \ell(\mathbf{w}(G)) \geq 0$  always holds, Lemma 5 tells us that the global clustering coefficient of a graph  $G$  is high whenever the angular distance between  $\mathbf{w}(G)$  and  $\mathbf{e}(G)$  is low. This relation to the global clustering coefficient shows that the wedge-vector indeed contains relevant information about our graph. However, if we would directly use the vector  $\mathbf{w}(G)$  as a query vector, we would run into a problem: because  $\mathbf{w}(G)$  is nonnegative, it always has a latitude that is at least  $\pi/2$ , while usually much higher than  $\pi/2$ . Therefore, the resulting Louvain candidate  $\mathcal{L}(\mathbf{w}(G))$  will likely have a latitude that is higher than desired, leading to very large communities.

The most straight-forward option would be to choose  $\lambda = \pi/2$  so that  $\mathbf{w}(G)$  is projected to the equator, leading to the query mapping  $\mathbf{q}_w(G) = \mathcal{P}_{\pi/2}(\mathbf{w}(G))$ . The motivation for this choice is that, by Lemma 4, the modularity vector has latitude  $\pi/2$  for the default resolution parameter value  $\gamma = 1$ . Thus, the projection to the equator is comparable to the most common form of modularity. Being on the equator implies that  $\langle \mathbf{q}_w(G), \mathbf{1} \rangle = 0$ . Then, the positive entries of  $\mathbf{q}_w(G)$  correspond to vertex-pairs that have more common neighbors than the graph average (over the vertex-pairs), while negative entries correspond to vertex-pairs that have less common neighbors than average. An approximate nearest neighbor of  $\mathbf{q}_w(G)$  will then correspond to a clustering where many of the intra-cluster pairs will have more common neighbors than average, while many of the inter-cluster pairs will have less common neighbors than average. However, note that for large graphs, a query vector on the equator will likely suffer from a similar resolution limit as  $q_M(G; \mathcal{N}, 1)$  for the same reason of discrepancy between the latitudes of the query vector and the ground truth clustering, as discussed in Section 4.

We emphasize that our framework enables a large class of new community detection methods, as compared to the modularity-based methods, by offering alternative queries, such as  $\mathbf{q}_w(G) = \mathcal{P}_{\pi/2}(\mathbf{w}(G))$ . The important advantage of this approach is that, in contrast to the modularity-based methods, a query vector does not need to be based on a particular null model. Instead, we may take a vector that contains information about the structure of the graph (such as the wedge-vector  $\mathbf{w}(G)$ ) and project it to a certain parallel (for example, the equator). Moreover, the resolution limit can be addressed by choosing the right latitude  $\lambda$ . In the next Section 6, we introduce a method that allows to tune the choice of  $\lambda$  to the network at hand.

## 6. A geometrically motivated clustering algorithm

Previously, we have discussed that the latitude of the query vector regulates the latitude of the resulting candidate clustering. Furthermore, in Section 4, we have seen that the latitude of the modularity vector is related to the resolution parameter. This tells us that the latitude of the modularity vector has to be adequately chosen to avoid problems like the resolution limit. Similarly, we have discussed that for the wedge-vector  $\mathbf{w}(G)$ , we also need to adjust its latitude in order to obtain a reasonable query vector. Thus, vectors such as  $\mathbf{e}(G)$  and  $\mathbf{w}(G)$  contain useful information for finding  $\mathbf{b}(T)$ , but their latitudes need to be adjusted in order to obtain a suitable query vector. In this section, we present the general setup where we are given an *input vector*  $\mathbf{x}$  that is presumed to contain useful information for detecting  $\mathbf{b}(T)$ , and we provide a latitude  $\lambda^*$  so that  $\mathbf{q}^*(\mathbf{x}) = \mathcal{P}_{\lambda^*}(\mathbf{x})$  is a suitable query vector.

This leads to a general geometric clustering algorithm that is not limited to community detection alone: our method can be used in any setting where such a pair-wise similarity vector  $\mathbf{x}$  is available, it need not have been derived from a network.

First, we introduce two properties that we empirically observed to hold in a wide range of situations. Next, we derive an algorithm that achieves desirable results whenever these observations are valid approximately.

### 6.1 Empirical observations

Because it is difficult to prove mathematical claims about the relation between a query vector and the resulting Louvain candidate, we rely on empirical observations instead. We formulate two empirical observations that will be useful for deriving our algorithm. These formulations capture some of the phenomena that came to our attention while performing experiments for a range of

query vectors, and they will be validated in Section 7. We note that these empirical observations are intentionally formulated in a way that is convenient for the derivation of our algorithm.

**Empirical Observation 1** *Whenever the correlation distance and the angular distance from the query vector  $\mathbf{q}$  to the ground truth clustering  $\mathbf{b}(T)$  are equal and smaller than the latitude of  $\mathbf{q}$ , then the correlation distance and angular distance between  $\mathbf{q}$  and the Louvain candidate  $\mathcal{L}(\mathbf{q})$  are approximately equal to this same value. That is, if  $d_{\text{CC}}(\mathbf{q}, \mathbf{b}(T)) = d_a(\mathbf{q}, \mathbf{b}(T)) < \ell(\mathbf{q})$ , then*

$$d_a(\mathbf{q}, \mathcal{L}(\mathbf{q})) \approx d_a(\mathbf{q}, \mathbf{b}(T)), \quad \text{and} \quad d_{\text{CC}}(\mathbf{q}, \mathcal{L}(\mathbf{q})) \approx d_{\text{CC}}(\mathbf{q}, \mathbf{b}(T)).$$

Empirical Observation 1 will be validated in Figures 3 and 4. We arrived at this formulation of the observation after varying the latitude  $\lambda$  of the query vector  $\mathbf{q} = \mathcal{P}_\lambda(\mathbf{x})$  and plotting four curves: the angular and correlation distances from  $\mathcal{P}_\lambda(\mathbf{x})$  to both  $\mathbf{b}(T)$  and  $\mathcal{L}(\mathcal{P}_\lambda(\mathbf{x}))$ , as a function of  $\lambda$ . We have observed that the four curves intersect each other at approximately the same value of  $\lambda$ . We tested this for several vectors  $\mathbf{x}$ , e.g.  $\mathbf{e}(G)$  or  $\mathbf{w}(G)$ , and for  $G$  generated by different random graph models (see Section 7 for more details). We added the condition  $d_a(\mathbf{q}, \mathbf{b}(T)) < \ell(\mathbf{q})$  because we observed that this phenomenon became less pronounced if  $d_a(\mathbf{q}, \mathbf{b}(T))$  is close to  $\ell(\mathbf{q})$  and is not visible at all for  $d_a(\mathbf{q}, \mathbf{b}(T)) > \ell(\mathbf{q})$ . The latter can be explained mathematically: the triangle inequality tells us that  $d_a(\mathbf{q}, \mathbf{b}(T)) \leq d_a(\mathbf{q}, \mathcal{L}(\mathbf{q})) + d_a(\mathcal{L}(\mathbf{q}), \mathbf{b}(T))$ . Then, using (16) and rewriting the result, we get

$$d_a(\mathcal{L}(\mathbf{q}), \mathbf{b}(T)) \geq d_a(\mathbf{q}, \mathbf{b}(T)) - \ell(\mathbf{q}).$$

Therefore, when the condition of Empirical Observation 1 is violated and  $d_a(\mathbf{q}, \mathbf{b}(T)) > \ell(\mathbf{q})$  holds, the right-hand side above is positive, so Louvain algorithm cannot possibly return a candidate clustering that is close to the true clustering.

We emphasize that Empirical Observation 1 is not a mathematical claim, but rather a rule of thumb that we observed to hold approximately in many settings and that will turn out to be useful in designing our algorithm. We are not yet able to explain *why* this observation holds so robustly, but the fact *that* it holds so robustly allows us to tune our algorithm accordingly.

Empirical Observation 1 plays a crucial role in the choice of the latitude of the query vector: one can imagine that if  $\mathbf{b}(T)$  and  $\mathcal{L}(\mathbf{q})$  are both at roughly equal distances from  $\mathbf{q}$  in both angular geometry and correlation-distance geometry, then  $\mathbf{b}(T)$  and  $\mathcal{L}(\mathbf{q})$  may also be similar in other aspects. Indeed, Theorem 7 will prove that in this case the difference between the latitudes of both vectors will be small. Furthermore, the experiments in Section 7 will show that the validation error  $d_{\text{CC}}(\mathcal{L}(\mathbf{q}), \mathbf{b}(T))$  is then also small. This tells us that it is desirable to have a query vector  $\mathbf{q}$  that satisfies the conditions of Empirical Observation 1. That is, we want to find a  $\mathbf{q}$  such that  $d_{\text{CC}}(\mathbf{q}, \mathbf{b}(T)) = d_a(\mathbf{q}, \mathbf{b}(T)) < \ell(\mathbf{q})$ . Given an input vector  $\mathbf{x}$ , Lemma 6 below will prove that there exists a latitude  $\lambda^*$ , as a function of  $\ell(\mathbf{b}(T))$  and  $d_{\text{CC}}(\mathbf{x}, \mathbf{b}(T))$ , such that  $\mathbf{q} = \mathcal{P}_{\lambda^*}(\mathbf{x})$  indeed satisfies these conditions.

Notice that computing this latitude  $\lambda^*$  to satisfy the conditions of Empirical Observation 1 requires knowledge of the ground truth latitude and its correlation distance to  $\mathbf{x}$ , which is often unavailable. The following empirical observation will be helpful in such situations:

**Empirical Observation 2** *For  $\lambda \in (0, \pi/2)$ ,  $\lambda \mapsto d_a(\mathcal{P}_\lambda(\mathbf{x}), \mathcal{L}(\mathcal{P}_\lambda(\mathbf{x})))$  and  $\lambda \mapsto d_{\text{CC}}(\mathcal{P}_\lambda(\mathbf{x}), \mathcal{L}(\mathcal{P}_\lambda(\mathbf{x})))$  intersect only once.*

Empirical Observation 2 is a combination of the observations that  $\lambda \mapsto d_a(\mathcal{P}_\lambda(\mathbf{x}), \mathcal{L}(\mathcal{P}_\lambda(\mathbf{x})))$  is roughly monotonous for  $\lambda \in (0, \pi/2)$ , while  $\lambda \mapsto d_{\text{CC}}(\mathcal{P}_\lambda(\mathbf{x}), \mathcal{L}(\mathcal{P}_\lambda(\mathbf{x})))$  is roughly constant on a relatively large interval around  $\lambda^*$ .

To summarize, Empirical Observation 1 can be read as stating that, as functions of the latitude  $\lambda$ , the four distances  $d_a(\mathcal{P}_\lambda(\mathbf{x}), \mathbf{b}(T))$ ,  $d_a(\mathcal{P}_\lambda(\mathbf{x}), \mathcal{L}(\mathcal{P}_\lambda(\mathbf{x})))$ ,  $d_{CC}(\mathcal{P}_\lambda(\mathbf{x}), \mathbf{b}(T))$  and  $d_{CC}(\mathcal{P}_\lambda(\mathbf{x}), \mathcal{L}(\mathcal{P}_\lambda(\mathbf{x})))$  roughly intersect at the same latitude  $\lambda^*$ . Now, Empirical Observation 2 tells us that  $d_a(\mathcal{P}_\lambda(\mathbf{x}), \mathcal{L}(\mathcal{P}_\lambda(\mathbf{x})))$  and  $d_{CC}(\mathcal{P}_\lambda(\mathbf{x}), \mathcal{L}(\mathcal{P}_\lambda(\mathbf{x})))$  only intersect once, so that this intersection will roughly coincide with the intersection of all four curves.

## 6.2 Formulation of the algorithm

Now we are ready to formulate the geometrically-motivated clustering algorithm. We assume that we are given an input vector  $\mathbf{x}$  that is positively correlated to the ground truth clustering  $\mathbf{b}(T)$  (i.e.  $d_{CC}(\mathbf{x}, \mathbf{b}(T)) < \pi/2$ ). The remainder of the algorithm consists of determining the query latitude  $\lambda^*$  and finding a candidate clustering  $\mathbf{b}(C)$  by minimizing the angular distance  $d_a(\mathcal{P}_{\lambda^*}(\mathbf{x}), \mathbf{b}(C))$ . This minimization step can be done by the Louvain algorithm or any other algorithm that is able to minimize this distance over the set of clusterings.

In choosing the latitude  $\lambda^*$ , we would ideally want to minimize the (correlation) distance between the resulting candidate  $\mathcal{L}(\mathcal{P}_{\lambda^*}(\mathbf{x}))$  and the ground truth. However, because the Louvain algorithm is too complex for such an analysis, we opt for a more modest goal. Namely, our aim instead is to choose the query vector latitude  $\lambda^*$  in such a way that the latitude of the Louvain candidate is approximately equal to the latitude of the ground truth vector. That is, our goal is to achieve

$$\ell(\mathcal{L}(\mathbf{q}^*(\mathbf{x}))) \approx \ell(\mathbf{b}(T)). \quad (18)$$

**Requiring partial knowledge of ground truth.** We present and analyze an approach to determining this  $\lambda^*$ . Our approach assumes some knowledge about the ground truth: we assume that its latitude  $\ell(\mathbf{b}(T))$  and its correlation distance  $d_{CC}(\mathbf{x}, \mathbf{b}(T))$  to our input vector are known or that approximations of these are available. At first, it might seem that requiring such knowledge about  $\mathbf{b}(T)$  would defeat the purpose of community detection. However, this is not uncommon in other community detection methods, such as likelihood-based methods (Newman, 2016; Prokhorenkova and Tikhonov, 2019). For instance, likelihood maximization using the Planted Partition Model, requires knowledge of the intra- and inter-community edge densities. These densities can be combined with the total density of the graph to compute the number of intra-community pairs  $m_T$ , which is related to  $\lambda_T$  by (9). This then allows us to compute the number of intra- and inter-community edges, from which  $d_{CC}(\mathbf{e}(G), \mathbf{b}(T))$  can be computed. We conclude that our method requires the *same* information as maximum-likelihood methods based on the Planted Partition Model or its degree-corrected variant. This suggests that requiring knowledge about  $\lambda_T$  and  $\theta$  is comparable to existing methods, and in particular, may thus be acceptable in practice.

**Latitude choice.** The candidate latitude choice is given by

$$\lambda^*(\lambda_T, \theta) = \arccos\left(\frac{\cos \lambda_T \cos \theta}{1 + \sin \lambda_T \sin \theta}\right), \quad (19)$$

where  $\lambda_T = \ell(\mathbf{b}(T))$  is the latitude of the ground truth clustering and  $\theta = d_{CC}(\mathbf{x}, \mathbf{b}(T))$  is the correlation distance to the input vector. The query vector of our algorithm will thus be given by

$$\mathbf{q}^*(\mathbf{x}) = \mathcal{P}_{\lambda^*(\ell(\mathbf{b}(T)), d_{CC}(\mathbf{x}, \mathbf{b}(T)))}(\mathbf{x}). \quad (20)$$

In summary, our geometrically-inspired community detection obtains a candidate clustering by evaluating the expression  $\mathcal{L}(\mathbf{q}^*(\mathbf{x}))$ , where the evaluation of  $\mathbf{q}^*(\mathbf{x})$  requires some partial knowledge of the ground truth.

In Sections 6.3 and 6.4, we provide mathematical justification for this algorithm. To this end, we will rely on Empirical Observation 1 as a black-box description of the Louvain algorithm: if we input a query vector that satisfies the conditions of Empirical Observation 1, then the resulting candidate clustering satisfies certain properties. In Lemma 6, we will prove that the conditions of Empirical Observation 1 are satisfied by the query vector  $\mathbf{q} = \mathbf{q}^*(\mathbf{x})$ , as given by (20). Furthermore, Theorem 7 will prove that the consequences of Empirical Observation 1 are sufficient to guarantee that the candidate indeed achieves the goal set in (18). The experiments of Section 7 will show that the exact latitude choice also roughly minimizes the correlation distance between the candidate and ground truth clustering. That is,  $\lambda^*$  approximately minimizes  $d_{\text{CC}}(\mathcal{L}(\mathcal{P}_\lambda(\mathbf{x})), \mathbf{b}(T))$ . Finally, in Section 6.5 we discuss how Empirical Observation 2 may be used to derive an iterative variant of our geometrically-inspired community detection that does not require partial knowledge of the ground truth clustering. However, the analysis of this iterative variant will be left for future research.

### 6.3 Analysis of the query latitude

We now prove that the query vector given in (20) indeed satisfies the conditions of Empirical Observation 1:

**Lemma 6** *Suppose  $\lambda_T = \ell(\mathbf{b}(T)) < \pi/2$  and  $\theta = d_{\text{CC}}(\mathbf{x}, \mathbf{b}(T)) < \pi/2$ . The query vector  $\mathbf{q}^*(\mathbf{x}) = \mathcal{P}_{\lambda^*(\lambda_T, \theta)}(\mathbf{x})$ , with  $\lambda^*$  given by (19) satisfies the conditions of Empirical Observation 1. That is,  $\lambda^*(\lambda_T, \theta) > d_a(\mathbf{q}^*(\mathbf{x}), \mathbf{b}(T)) = d_{\text{CC}}(\mathbf{q}^*(\mathbf{x}), \mathbf{b}(T)) = \theta$ .*

**Proof** Note that for any  $\lambda \in (0, \pi)$ , we have  $d_{\text{CC}}(\mathcal{P}_\lambda(\mathbf{x}), \mathbf{b}(T)) = d_{\text{CC}}(\mathbf{x}, \mathbf{b}(T)) = \theta$ , as the parallel projection is a projection along the meridian, so that the choice of  $\lambda$  will not affect the correlation distance to the ground truth vector. Thus, we only have to find the latitude for which  $d_a(\mathcal{P}_\lambda(\mathbf{x}), \mathbf{b}(T)) = \theta$  holds. Figure 2 illustrates the geometric construction by which we will derive the desired latitude  $\lambda^*$ : first we find  $\lambda'$  such that  $\mathcal{P}_{\lambda'}(\mathbf{x})$  minimizes the angular distance to  $\mathbf{b}(T)$ . Then we compute  $d\lambda$  so that the points  $\mathcal{P}_{\lambda'-d\lambda}(\mathbf{x})$  and  $\mathcal{P}_{\lambda'+d\lambda}(\mathbf{x}) = \mathbf{q}^*(\mathbf{x})$  are both at angular distance  $\theta$  from  $\mathbf{b}(T)$ .

In more detail, consider the great circle  $(\mathcal{P}_\lambda(\mathbf{x}))_{\lambda \in (-\pi, \pi]}$  that is formed by extending the meridian of  $\mathbf{x}$  by its opposite meridian. Since the angular distance between  $\mathbf{b}(T)$  and the nearest point on this great circle is less<sup>2</sup> than the correlation distance  $\theta$ , there must be precisely two points on this great circle that are at angular distance  $\theta$  from  $\mathbf{b}(T)$ . Let  $\lambda_1$  and  $\lambda_2$  denote the latitudes of these points. Now  $\mathcal{P}_{\lambda_1}(\mathbf{x}), \mathcal{P}_{\lambda_2}(\mathbf{x})$  and  $\mathbf{b}(T)$  form a hyperspherical isosceles triangle. This implies that the point at latitude  $\lambda' = \frac{1}{2}(\lambda_1 + \lambda_2)$  minimizes the distance to  $\mathbf{b}(T)$  over the great circle and that the line from  $\mathbf{b}(T)$  to  $\mathcal{P}_{\lambda'}(\mathbf{x})$  is perpendicular to our great circle. Therefore, the points  $-\mathbf{1}, \mathbf{b}(T)$  and  $\mathcal{P}_{\lambda'}(\mathbf{x})$  form a hyperspherical right-angled triangle. This allows us to use the right-angle formulae, as given in (7), to compute  $\lambda' = d_a(-\mathbf{1}, \mathcal{P}_{\lambda'}(\mathbf{x}))$  and  $d_a(\mathbf{b}(T), \mathcal{P}_{\lambda'}(\mathbf{x}))$ . To compute  $d_a(\mathcal{P}_{\lambda'}(\mathbf{x}), \mathbf{b}(T))$ , we rewrite  $\sin \theta = \sin \angle(\mathcal{P}_{\lambda'}(\mathbf{x}), -\mathbf{1}, \mathbf{b}(T))$  as

$$\sin \theta = \frac{\sin d_a(\mathcal{P}_{\lambda'}(\mathbf{x}), \mathbf{b}(T))}{\sin d_a(-\mathbf{1}, \mathbf{b}(T))} = \frac{\sin d_a(\mathcal{P}_{\lambda'}(\mathbf{x}), \mathbf{b}(T))}{\sin \lambda_T},$$

which gives  $\sin d_a(\mathcal{P}_{\lambda'}(\mathbf{x}), \mathbf{b}(T)) = \sin \theta \sin \lambda_T$ , with corresponding cosine  $\cos d_a(\mathcal{P}_{\lambda'}(\mathbf{x}), \mathbf{b}(T)) = \sqrt{1 - \sin^2 \theta \sin^2 \lambda_T}$ . To compute  $\lambda'$ , we rewrite the right-angle formula of  $\cos \theta$  (see (7)) to

$$\cos \theta = \frac{\tan d_a(-\mathbf{1}, \mathcal{P}_{\lambda'}(\mathbf{x}))}{\tan d_a(-\mathbf{1}, \mathbf{b}(T))} = \frac{\tan \lambda'}{\tan \lambda_T},$$

---

2. For the equator point  $\mathcal{P}_{\pi/2}(\mathbf{b}(T))$ , these distances would be equal. However, since we assumed  $\lambda_T < \pi/2$ , the angular distance to the meridian of  $\mathbf{x}$  is strictly smaller.

which gives  $\tan \lambda' = \cos \theta \tan \lambda_T$ .

Let us define  $d\lambda = |\lambda' - \lambda_1| = |\lambda' - \lambda_2|$ . As  $\mathbf{b}(T)$ ,  $\mathcal{P}_{\lambda'}(\mathbf{x})$  and  $\mathcal{P}_{\lambda_1}(\mathbf{x})$  also form a hyperspherical right-angled triangle, this allows us to use the hyperspherical Pythagorean theorem, as given in (6), to compute  $d\lambda$  from

$$\cos(d_a(\mathcal{P}_{\lambda'}(\mathbf{x}), \mathbf{b}(T))) \cos(d\lambda) = \cos \theta.$$

Therefore,

$$\cos(d\lambda) = \frac{\cos \theta}{\cos d_a(\mathcal{P}_{\lambda'}(\mathbf{x}), \mathbf{b}(T))} = \frac{\cos \theta}{\sqrt{1 - \sin^2 \lambda_T \sin^2 \theta}}.$$

In turn, this implies that  $\lambda_1, \lambda_2$  are given by

$$\lambda' \pm d\lambda = \arctan(\cos \theta \tan \lambda_T) \pm \arccos \left( \frac{\cos \theta}{\sqrt{1 - \sin^2 \lambda_T \sin^2 \theta}} \right). \quad (21)$$

We take its cosine and rewrite it to

$$\begin{aligned} \cos(\lambda' \pm d\lambda) &= \cos \left( \arctan(\cos \theta \tan \lambda_T) \pm \arccos \left( \frac{\cos \theta}{\sqrt{1 - \sin^2 \lambda_T \sin^2 \theta}} \right) \right) \\ &= \cos(\arctan(\cos \theta \tan \lambda_T)) \frac{\cos \theta}{\sqrt{1 - \sin^2 \lambda_T \sin^2 \theta}} \\ &\quad \mp \sin(\arctan(\cos \theta \tan \lambda_T)) \sin \left( \arccos \left( \frac{\cos \theta}{\sqrt{1 - \sin^2 \lambda_T \sin^2 \theta}} \right) \right) \\ &= \frac{1}{\sqrt{1 + \cos^2 \theta \tan^2 \lambda_T}} \frac{\cos \theta}{\sqrt{1 - \sin^2 \lambda_T \sin^2 \theta}} \\ &\quad \mp \frac{\cos \theta \tan \lambda_T}{\sqrt{1 + \cos^2 \theta \tan^2 \lambda_T}} \sqrt{1 - \left( \frac{\cos \theta}{\sqrt{1 - \sin^2 \lambda_T \sin^2 \theta}} \right)^2} \\ &= \frac{\cos \lambda_T}{\sqrt{\cos^2 \lambda_T + \cos^2 \theta \sin^2 \lambda_T}} \frac{\cos \theta}{\sqrt{1 - \sin^2 \lambda_T \sin^2 \theta}} \\ &\quad \mp \frac{\cos \theta \sin \lambda_T}{\sqrt{\cos^2 \lambda_T + \cos^2 \theta \sin^2 \lambda_T}} \sqrt{\frac{\sin^2 \theta \cos^2 \lambda_T}{1 - \sin^2 \lambda_T \sin^2 \theta}} \\ &= \frac{\cos \lambda_T}{\sqrt{1 - \sin^2 \lambda_T \sin^2 \theta}} \frac{\cos \theta}{\sqrt{1 - \sin^2 \lambda_T \sin^2 \theta}} \\ &\quad \mp \frac{\cos \theta \sin \lambda_T}{\sqrt{1 - \sin^2 \lambda_T \sin^2 \theta}} \frac{\sin \theta \cos \lambda_T}{\sqrt{1 - \sin^2 \lambda_T \sin^2 \theta}} \\ &= \frac{\cos \lambda_T \cos \theta (1 \mp \sin \lambda_T \sin \theta)}{1 - \sin^2 \lambda_T \sin^2 \theta} \\ &= \frac{\cos \lambda_T \cos \theta}{1 \pm \sin \lambda_T \sin \theta}. \end{aligned}$$

We see that  $\lambda' + d\lambda = \lambda^*$ , as given by (19).

The last condition that needs to be verified is  $\lambda > \theta$ , or equivalently,  $\cos \lambda < \cos \theta$ . We show that  $\lambda^* = \lambda' + d\lambda$  satisfies this condition while  $\lambda' - d\lambda$  does not necessarily satisfy it. Since  $\lambda_T < \pi/2$ , we have

$$\cos \lambda^* = \frac{\cos \lambda_T \cos \theta}{1 + \sin \lambda_T \sin \theta} < \cos \theta.$$

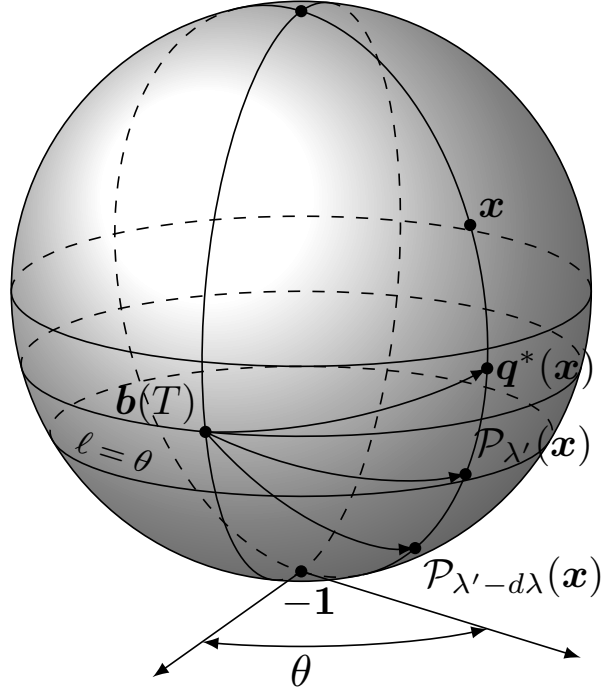


Figure 2: Illustration of the query latitude for an input vector  $\mathbf{x}$  in the three-dimensional subspace spanned by  $\mathbf{x}, \mathbf{b}(T), -\mathbf{1}$ . The solid arcs are on the visible side of the sphere while the dashed arcs are on the back side. For this illustration, we have used  $\lambda_T = \ell(\mathbf{b}(T)) = \frac{5}{12}\pi$ . The angles  $\lambda'$  and  $d\lambda$  are as described in the proof of Lemma 6 and  $\mathbf{q}^*(\mathbf{x}) = \mathcal{P}_{\lambda'+d\lambda}(\mathbf{x})$ . The parallels with latitudes  $\theta, \lambda_T$  and  $\pi/2$  are drawn. Lemma 6 tells us that  $d_a(\mathbf{q}^*(\mathbf{x}), \mathbf{b}(T)) = d_a(\mathcal{P}_{\lambda'-d\lambda}(\mathbf{x}), \mathbf{b}(T)) = \theta$  and  $\lambda' + d\lambda > \theta$  while  $\lambda' - d\lambda > \theta$  generally doesn't hold.

Thus,  $\lambda^* = \lambda' + d\lambda$  indeed satisfies the conditions of Empirical Observation 1. ■

Note that the proof of Lemma 6 (and the corresponding illustration Figure 2) also gives a second solution  $\mathcal{P}_{\lambda'-d\lambda}(\mathbf{x})$ . However, this solution does not generally satisfy the condition  $\lambda' - d\lambda > \theta$ . It only satisfies this condition whenever  $\cos(\lambda' - d\lambda) < \cos \theta$ , which can be rewritten to

$$\sin \theta < \frac{1 - \cos \lambda_T}{\sin \lambda_T} = \tan \left( \frac{\lambda_T}{2} \right).$$

Hence, the admissibility of this second solution depends on the particular values of  $\theta$  and  $\lambda_T$ . However, in the cases of our interest,  $\lambda_T$  is small compared to  $\theta$  (recall (10)) so that this alternative latitude will generally not satisfy the conditions of Empirical Observation 1.

#### 6.4 Analysis of the candidate latitude

Lemma 6 tells us that the query vector  $\mathbf{q}^*(\mathbf{x}) = \mathcal{P}_{\lambda^*}(\mathbf{x})$ , with latitude  $\lambda^*$  as defined by (19) satisfies the conditions of Empirical Observation 1. We now show that if the consequences of Empirical Observation 1 hold, that then the Louvain candidate has approximately the same latitude as the ground truth:

**Theorem 7** *Suppose  $d_{\text{CC}}(\mathbf{q}^*, \mathbf{b}(T)) = \theta < \pi/2$  and  $\lambda_T = \ell(\mathbf{b}(T))$  and suppose that*

$$d_a(\mathbf{q}^*, \mathcal{L}(\mathbf{q}^*)) = \theta + \varepsilon_a, \quad \text{and} \quad d_{\text{CC}}(\mathbf{q}^*, \mathcal{L}(\mathbf{q}^*)) = \theta + \varepsilon_{\text{CC}},$$

for  $\varepsilon_a, \varepsilon_{CC}$  small, and a query vector  $\mathbf{q}^*$  with latitude  $\lambda^*(\lambda_T, \theta)$  as given by (19). Then the latitude of the candidate clustering can be approximated as

$$\ell(\mathcal{L}(\mathbf{q}^*)) = \lambda_T - \varepsilon_a \frac{1 + \sin \lambda_T \sin \theta}{\cos \lambda_T \cos \theta} + \varepsilon_{CC} \frac{\sin \lambda_T (\sin \theta + \sin \lambda_T)}{\cos \lambda_T \cos \theta} + \mathcal{O}(\varepsilon_{CC}^2 + \varepsilon_{CC} \varepsilon_a + \varepsilon_a^2). \quad (22)$$

**Proof** Let  $\lambda_C = \ell(\mathcal{L}(\mathbf{q}^*))$  and let  $\Lambda = \angle(\mathcal{L}(\mathbf{q}^*), \mathbf{q}^*, -1)$ . We rewrite  $\cos \Lambda$  using the cosine rule. This gives

$$\cos \Lambda = \frac{\cos \lambda_C - \cos(\theta + \varepsilon_a) \cos \lambda^*}{\sin(\theta + \varepsilon_a) \sin \lambda^*}. \quad (23)$$

We use  $\cos \Lambda = \cos \lambda_C + (\cos \Lambda - \cos \lambda_C)$  to rewrite (23) to

$$\cos \lambda_C = \frac{\cos(\theta + \varepsilon_a) \cos \lambda^*}{1 - \sin(\theta + \varepsilon_a) \sin \lambda^*} + (\cos \Lambda - \cos \lambda_C) \frac{\sin(\theta + \varepsilon_a) \sin \lambda^*}{1 - \sin(\theta + \varepsilon_a) \sin \lambda^*}.$$

We substitute  $\lambda^*$  as given by (19), to obtain

$$\begin{aligned} \cos \lambda_C &= \frac{\cos(\theta + \varepsilon_a) \cos \theta \cos \lambda_T}{1 + \sin \theta \sin \lambda_T - \sin(\theta + \varepsilon_a)(\sin \theta + \sin \lambda_T)} \\ &\quad + (\cos \Lambda - \cos \lambda_C) \frac{\sin(\theta + \varepsilon_a)(\sin \theta + \sin \lambda_T)}{1 + \sin \theta \sin \lambda_T - \sin(\theta + \varepsilon_a)(\sin \theta + \sin \lambda_T)}. \end{aligned}$$

The first term can be approximated by a first-order Taylor polynomial around  $\varepsilon_a = 0$ . This gives

$$\frac{\cos(\theta + \varepsilon_a) \cos \theta \cos \lambda_T}{1 + \sin \theta \sin \lambda_T - \sin(\theta + \varepsilon_a)(\sin \theta + \sin \lambda_T)} = \cos \lambda_T + \varepsilon_a \frac{\cos \lambda_T \sin \lambda_T}{\cos \theta} + \mathcal{O}(\varepsilon_a^2).$$

Next, we approximate  $\cos \Lambda - \cos \lambda_C$ . The sine rule tells us that

$$\frac{\sin \Lambda}{\sin \lambda_C} = \frac{\sin d_{CC}(\mathcal{L}(\mathbf{q}^*), \mathbf{q}^*)}{\sin d_a(\mathcal{L}(\mathbf{q}^*), \mathbf{q}^*)} = \frac{\sin(\theta + \varepsilon_{CC})}{\sin(\theta + \varepsilon_a)}.$$

This can be rewritten to

$$\cos \Lambda = \sqrt{1 - \frac{\sin^2(\theta + \varepsilon_{CC})}{\sin^2(\theta + \varepsilon_a)} \sin^2 \lambda_C}.$$

Its first-order Taylor expansion around  $\varepsilon_{CC} = \varepsilon_a = 0$  is given by

$$\cos \Lambda = \cos \lambda_C - \frac{\sin^2 \lambda_C}{\cos \lambda_C \tan \theta} (\varepsilon_{CC} - \varepsilon_a) + \mathcal{O}(\varepsilon_{CC}^2 + \varepsilon_{CC} \varepsilon_a + \varepsilon_a^2).$$

We see that  $\cos \Lambda - \cos \lambda_C = \mathcal{O}(\varepsilon_{CC} + \varepsilon_{CC} \varepsilon_a + \varepsilon_a)$ , so that the zeroth order approximation  $\varepsilon_a \approx 0$  is sufficient for the remaining factor. Combining all of these, we get

$$\cos \lambda_C = \cos \lambda_T + \varepsilon_a \frac{\cos \lambda_T \sin \lambda_T}{\cos \theta} + (\varepsilon_a - \varepsilon_{CC}) \frac{\sin^2 \lambda_C}{\cos \lambda_C \tan \theta} \frac{\sin \theta (\sin \theta + \sin \lambda_T)}{\cos^2 \theta} + \mathcal{O}(\varepsilon_{CC}^2 + \varepsilon_{CC} \varepsilon_a + \varepsilon_a^2),$$

which can be rewritten to

$$\cos \lambda_C = \cos \lambda_T + \varepsilon_a \frac{\cos \lambda_T \sin \lambda_T}{\cos \theta} + (\varepsilon_a - \varepsilon_{CC}) \frac{\sin^2 \lambda_C}{\cos \lambda_C \tan \theta} \frac{\sin \theta (\sin \theta + \sin \lambda_T)}{\cos^2 \theta} + \mathcal{O}(\varepsilon_{CC}^2 + \varepsilon_{CC} \varepsilon_a + \varepsilon_a^2). \quad (24)$$

Note that (24) can be substituted into itself to obtain

$$\cos \lambda_C = \cos \lambda_T + \varepsilon_a \frac{\sin \lambda_T + \sin^2 \lambda_T \sin \theta}{\cos \lambda_T \cos \theta} - \varepsilon_{CC} \frac{\sin^2 \lambda_T (\sin \theta + \sin \lambda_T)}{\cos \lambda_T \cos \theta} + O(\varepsilon_{CC}^2 + \varepsilon_{CC} \varepsilon_a + \varepsilon_a^2). \quad (25)$$

Now we only need to take the arccosine of this expression. The Taylor expansion of  $\arccos(x)$  around  $x = \cos \lambda_T$  is given by

$$\arccos(x) = \lambda_T - \frac{x - \cos \lambda_T}{\sin \lambda_T} + \mathcal{O}((x - \cos \lambda_T)^2). \quad (26)$$

Finally, we substitute (25) into (26) to get

$$\lambda_C = \lambda_T - \varepsilon_a \frac{1 + \sin \lambda_T \sin \theta}{\cos \lambda_T \cos \theta} + \varepsilon_{CC} \frac{\sin \lambda_T (\sin \theta + \sin \lambda_T)}{\cos \lambda_T \cos \theta} + O(\varepsilon_{CC}^2 + \varepsilon_{CC} \varepsilon_a + \varepsilon_a^2). \quad \blacksquare$$

From the  $\cos \lambda_T \cos \theta$  in the denominator of (22), we see that the error may be large whenever  $\theta$  or  $\lambda_T$  is close to  $\pi/2$ . Note that  $\cos \theta = \cos d_{CC}(\mathbf{x}, \mathbf{b}(T))$  is the linear correlation between the vectors  $\mathbf{x}$  and  $\mathbf{b}(T)$ . Therefore,  $\theta = \pi/2$  means that  $\mathbf{q}^*$  and  $\mathbf{b}(T)$  are uncorrelated. In such cases, it is understandable that the algorithm does not lead to a good candidate clustering as the vector  $\mathbf{x}$  simply does not contain enough useful information about the desired community structure. As we have seen in (10),  $\lambda_T$  tends to be small in practice so that  $\lambda_T \approx \pi/2$  will generally not occur in large-scale applications.

**Correlation distance as a difficulty measure.** From Theorem 7, we see that the performance of our algorithm depends on the correlation distance  $\theta = d_{CC}(\mathbf{x}, \mathbf{b}(T))$  since the discrepancy between the candidate latitude and true latitude  $|\lambda_T - \lambda_C|$  is large when  $\theta$  is large. Furthermore, the triangle inequality tells us that

$$d_{CC}(\mathbf{b}(T), \mathbf{b}(C)) \leq d_{CC}(\mathbf{q}^*(\mathbf{x}), \mathbf{b}(C)) + d_{CC}(\mathbf{q}^*(\mathbf{x}), \mathbf{b}(T)) = 2\theta + \varepsilon_{CC}, \quad (27)$$

which provides a performance guarantee where better performance is guaranteed when  $\theta$  is small. In the extreme case where  $\theta = 0$ , (19) gives  $\lambda^* = \lambda_T$ , i.e.,  $\mathbf{q}^*$  lies on the same meridian and parallel as  $\mathbf{b}(T)$  which means that  $\mathbf{q}^*(\mathbf{x}) = \mathbf{b}(T)$ . Since  $\mathcal{L}$  is a projection onto the set of clustering vectors (recall Lemma 9), we also have  $\mathcal{L}(\mathbf{q}^*(\mathbf{x})) = \mathbf{b}(T)$  so that perfect recovery of the communities is guaranteed. We thus see that the correlation distance between the ground truth clustering vector  $\mathbf{b}(T)$  and the input vector  $\mathbf{x}$  is a useful measure of how well  $\mathbf{x}$  can be used to detect the communities  $T$ . Previously, we have seen that the correlation distance  $d_{CC}(\mathbf{b}(T), \mathbf{b}(C))$  is also a suitable measure of the similarity between the clusterings  $T$  and  $C$ , which shows the importance of the correlation distance.

## 6.5 An iterative alternative without requiring ground-truth knowledge

We thus utilized Empirical Observation 1 to develop a geometrically-inspired community detection method that requires partial knowledge of the ground truth. In this section, we will briefly discuss how Empirical Observation 2 may be used to develop a variant of this community detection method that does not require such knowledge of the ground truth. However, we leave the analysis of this method to future work.

Recall that the query latitude  $\lambda^*$ , as given in (19), was chosen to correspond to the intersection point of  $\lambda \mapsto d_a(\mathcal{P}_\lambda(\mathbf{x}), \mathbf{b}(T))$  with  $\lambda \mapsto d_{CC}(\mathcal{P}_\lambda(\mathbf{x}), \mathbf{b}(T))$ . Empirical Observation 1 tells us that

for this  $\lambda^*$  the approximations  $d_a(\mathcal{P}_\lambda(\mathbf{x}), \mathbf{b}(T)) \approx d_a(\mathcal{P}_\lambda(\mathbf{x}), \mathcal{L}(\mathcal{P}_\lambda(\mathbf{x})))$  and  $d_{CC}(\mathcal{P}_\lambda(\mathbf{x}), \mathbf{b}(T)) \approx d_{CC}(\mathcal{P}_\lambda(\mathbf{x}), \mathcal{L}(\mathcal{P}_\lambda(\mathbf{x})))$  are valid. Thus, we can expect that this  $\lambda^*$  also roughly corresponds to an intersection of  $\lambda \mapsto d_a(\mathcal{P}_\lambda(\mathbf{x}), \mathcal{L}(\mathcal{P}_\lambda(\mathbf{x})))$  with  $\lambda \mapsto d_{CC}(\mathcal{P}_\lambda(\mathbf{x}), \mathcal{L}(\mathcal{P}_\lambda(\mathbf{x})))$ . In turn, Empirical Observation 2 tells us that these latter two only intersect once, so that if we define  $\hat{\lambda}$  as the intersection between  $\lambda \mapsto d_a(\mathcal{P}_\lambda(\mathbf{x}), \mathcal{L}(\mathcal{P}_\lambda(\mathbf{x})))$  and  $\lambda \mapsto d_{CC}(\mathcal{P}_\lambda(\mathbf{x}), \mathcal{L}(\mathcal{P}_\lambda(\mathbf{x})))$ , then we can expect  $\hat{\lambda} \approx \lambda^*$  to hold. Crucially, finding  $\hat{\lambda}$  does not require knowledge of  $\ell(\mathbf{b}(T))$  or  $d_{CC}(\mathbf{x}, \mathbf{b}(T))$  as we simply need to find the root of  $\lambda \mapsto d_a(\mathcal{P}_\lambda(\mathbf{x}), \mathcal{L}(\mathcal{P}_\lambda(\mathbf{x}))) - d_{CC}(\mathcal{P}_\lambda(\mathbf{x}), \mathcal{L}(\mathcal{P}_\lambda(\mathbf{x})))$ . To this end,  $\hat{\lambda}$  can be found by any root-finding algorithm such as the bisection (a.k.a. binary search) method.

Note that each evaluation of  $d_a(\mathcal{P}_\lambda(\mathbf{x}), \mathcal{L}(\mathcal{P}_\lambda(\mathbf{x}))) - d_{CC}(\mathcal{P}_\lambda(\mathbf{x}), \mathcal{L}(\mathcal{P}_\lambda(\mathbf{x})))$  requires performing the Louvain algorithm, so that this approach would be computationally more expensive than the original method introduced in Section 6.2. The analysis of this iterative community detection algorithm would also be significantly more involved than that of the original algorithm: in Theorem 7 we were able to express the difference between candidate and ground truth latitude in terms of the errors  $\varepsilon_a$  and  $\varepsilon_{CC}$ , which were known as we required the values  $d_a(\mathbf{q}^*(\mathbf{x}), \mathbf{b}(T))$  and  $d_{CC}(\mathbf{q}^*(\mathbf{x}), \mathbf{b}(T))$  to be known and equal. However, for the iterative variant, the only error term that we could work with is  $d_a(\mathcal{P}_\lambda(\mathbf{x}), \mathcal{L}(\mathcal{P}_\lambda(\mathbf{x}))) - d_{CC}(\mathcal{P}_\lambda(\mathbf{x}), \mathcal{L}(\mathcal{P}_\lambda(\mathbf{x})))$ , and it would be unlikely that a similar expression could be obtained in terms of this error alone. For these reasons, we leave the analysis of this iterative variant to future work.

## 7. Experiments

In this section we validate Observations 1 and 2, and evaluate the community detection methods that have been introduced in Sections 5 and 6, using experiments on random graphs with a known ground truth community structure.

**Validating the empirical observations.** In Figures 3 and 4, we validate Observations 1 and 2 for  $\mathbf{x} \in \{\mathbf{e}(G), \mathbf{w}(G)\}$ , where  $G$  is a random graph drawn from a Planted Partition Model (PPM). The PPM is a Stochastic Block Model where the block matrix has diagonal entries equal to the intra-community density  $p_{\text{in}}$  while off-diagonal entries are equal to the inter-community density  $p_{\text{out}}$ . For Figures 3 and 4,  $p_{\text{in}}$  and  $p_{\text{out}}$  are chosen to set the desired expected number of intra- and inter-community neighbors.

Empirical Observation 1 claims that the distances  $d_a(\mathcal{P}_\lambda(\mathbf{x}), \mathbf{b}(T))$ ,  $d_a(\mathcal{P}_\lambda(\mathbf{x}), \mathcal{L}(\mathcal{P}_\lambda(\mathbf{x})))$  and  $d_{CC}(\mathcal{P}_\lambda(\mathbf{x}), \mathcal{L}(\mathcal{P}_\lambda(\mathbf{x})))$  as functions of  $\lambda$  roughly intersect the point  $(\lambda^*, d_{CC}(\mathbf{x}, \mathbf{b}(T)))$ , which is marked by a red cross in the Figures 3a, 3c, 4a and 4c. We see that in three out of four cases, the lines intersect the cross almost exactly, while only in Figure 4a the cross is visibly missed. For this last case, this larger discrepancy can be explained by the fact that only half of the edges are intra-community edges so that  $\mathbf{e}(G)$  provides less useful information for detecting  $\mathbf{b}(T)$ , which is also reflected in the fact that the correlation distance  $d_{CC}(\mathbf{e}(G), \mathbf{b}(T))$  is slightly larger than in the other experiments.

**Validating the algorithm.** Theorem 7 tells us that the quality of the approximation  $\ell(\mathcal{L}(\mathbf{q}^*(\mathbf{x}))) \approx \ell(\mathbf{b}(T))$  depends on the quality of the approximations of Empirical Observation 1. In Figures 3b, 3d, 4b and 4d, the latitudes of the candidates are plotted while the point  $(\lambda^*, \ell(\mathbf{b}(T)))$  is marked with a cross. We see that the candidate latitudes indeed roughly intersect the cross in three out of four figures while in Figure 4b, it is clearly missed. This supports the claim that the quality of the approximation  $\ell(\mathcal{L}(\mathbf{q}^*(\mathbf{x}))) \approx \ell(\mathbf{b}(T))$  depends on the quality of the approximations of Empirical Observation 1. In these same figures, we also plot the correlation distance between the candidate clusterings and the ground truth clusterings, which serves as a validation measure for the community detection results. We see that this distance is minimized roughly around the latitude  $\lambda^*$ . We

emphasize that our algorithm was not designed to directly minimize this correlation distance, but was merely tuned to obtain candidates of roughly the right latitude. Hence, though it is positive that the tuning seems to roughly minimize the correlation distance, the presented theoretical results are not able to guarantee it.

We thus verified the empirical observations and the resulting community detection methods for a number of graphs drawn from PPMs with varying parameters. When repeating these experiments for the Degree-Corrected Stochastic Block Models (DCSBMs), the results are similar. Note that it is infeasible to perform this validation in a way that it is representative for *all* networks on which community detection may be applied.

**Comparison to likelihood maximization.** In Figures 5, 6 and 7, we compare the performances of our novel detection methods to existing modularity-based methods on Planted Partition Models with different numbers of communities. In each of these figures, we vary the fraction of the edges that connect vertices of different communities. The following query mappings are used:  $\mathbf{q}_e(G) = \mathcal{P}_{\pi/2}(\mathbf{e}(G))$  corresponds to ER-modularity with the resolution parameter set to 1,  $\mathbf{q}_e^{(\text{MLE})}$  corresponds to ER-modularity with the resolution parameter set to the value for which equivalence with PPM Maximum Likelihood Estimation is achieved,  $\mathbf{q}_w$  is as introduced in Section 5 while  $\mathbf{q}_e^*(G) = \mathbf{q}^*(\mathbf{e}(G))$  and  $\mathbf{q}_w^*(G) = \mathbf{q}^*(\mathbf{w}(G))$  correspond to our geometrically-inspired community detection method, as introduced in Section 6.

Similarly, Figure 8 compares the performances of our detection methods to existing modularity-based methods on a DCSBM with degrees following a power law. The following query mappings are used:  $\mathbf{q}_e^{(\text{MLE})}$  is again the PPM-MLE,  $\mathbf{q}_e^*$  and  $\mathbf{q}_w^*$  again correspond to our method applied to the edge-connectivity vector  $\mathbf{e}(G)$  and wedge-vector  $\mathbf{w}(G)$  respectively,  $\mathbf{q}_d^{(\text{MLE})}$  corresponds to the DCSBM maximum likelihood estimator (which corresponds to CM-modularity  $\mathbf{q}_M(G; \text{CM}, \gamma_{(\text{MLE})})$  for some  $\gamma_{(\text{MLE})}$ ), and  $\mathbf{q}_d^*$  is our method applied to the CM-modularity-vector  $\mathbf{q}_M(G; \text{CM}, 1)$ .

We now discuss the results. First of all, it can be seen in Figures 5, 6 and 7 that the query mappings  $\mathbf{q}_e^*$  and  $\mathbf{q}_w^*$  consistently outperform their unadjusted counterparts  $\mathbf{q}_e$  and  $\mathbf{q}_w$ , which tells us that the latitude-tuning has a positive effect. In Figure 8, the unadjusted query mappings  $\mathbf{q}_e$  and  $\mathbf{q}_w$  are left out to prevent cluttering the image.

We see that for PPM graphs,  $\mathbf{q}_e^*$  achieves similar results in terms of correlation distance as  $\mathbf{q}_e^{(\text{MLE})}$ , while for DCSBM graphs,  $\mathbf{q}_d^*$  achieves similar results as  $\mathbf{q}_d^{(\text{MLE})}$ . This is remarkable, as it was previously argued that likelihood-based methods are optimal when using the true likelihood function Newman (2016), while our general method seems to perform equally well.

Moreover, Figures 5b, 6b, 7b and 8b show that the candidates obtained through our method generally have a latitude that is closer to the true value than those obtained from maximizing the likelihood. When a large fraction of the edges are inter-community edges, we even see that maximizing the true likelihood function consistently leads to candidates with too low latitude. This suggests that optimizing likelihood may be slightly *biased* towards candidates with lower latitude.

Finally, we see that for 40 and 20 communities (see Figures 5a and 6a), the edge-based query mappings  $\mathbf{q}_w^*$  and  $\mathbf{q}_e^{(\text{MLE})}$  outperform the wedge-based query mapping  $\mathbf{q}_w^*$ , while for 10 communities (see Figure 7a), the wedge-based query mapping  $\mathbf{q}_w^*$  outperforms the edge-based mappings. This could be explained by the fact that wedge-based vectors count paths of length 2 (as opposed to 1 for edge-based). On the one hand, when a community is large, paths of length 1 may only reach a small fraction of the community nodes while paths of length 2 will reach a larger fraction of the community. On the other hand, when communities are small, this 2-neighborhood will contain many vertices outside its community. Thus, we see that for some graphs, choosing a different input vector can even lead to strictly better performance than likelihood-based methods. This shows the advantage of the flexibility of the geometric framework.

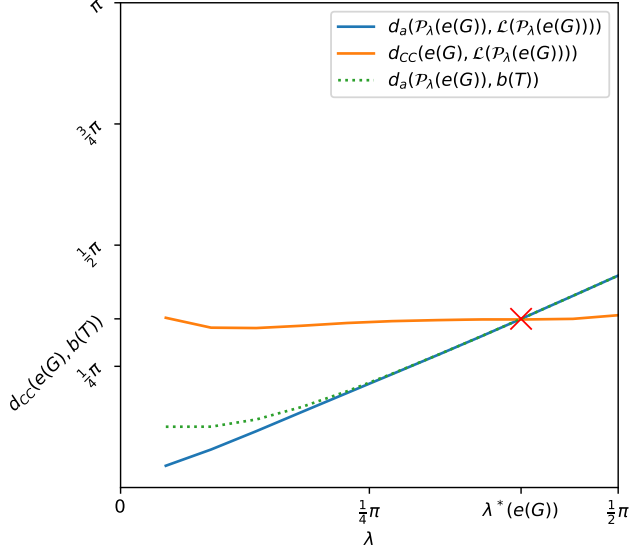
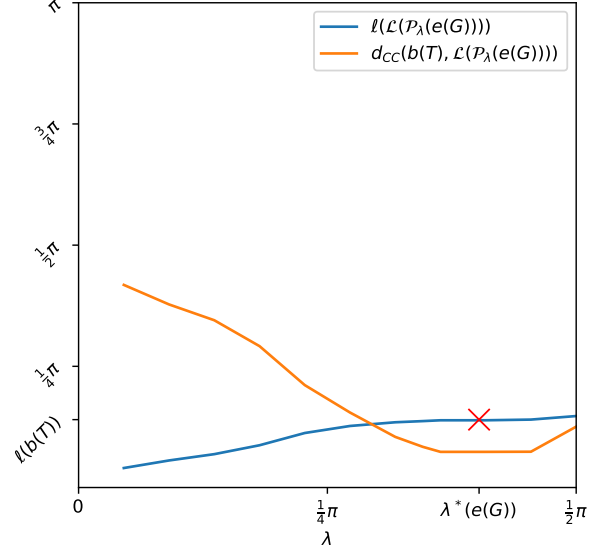
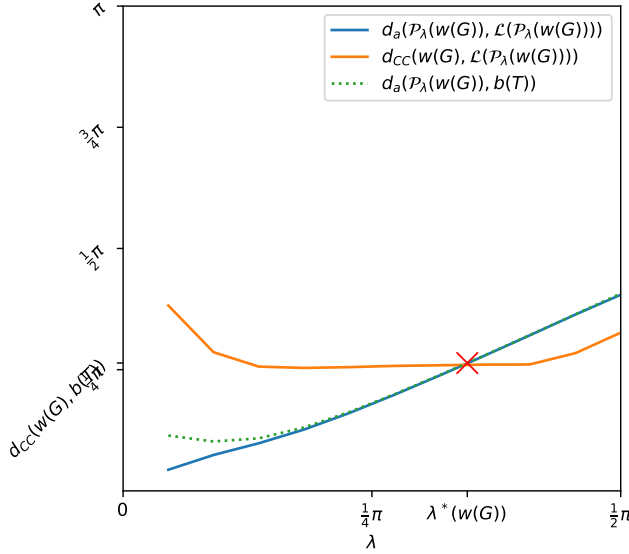
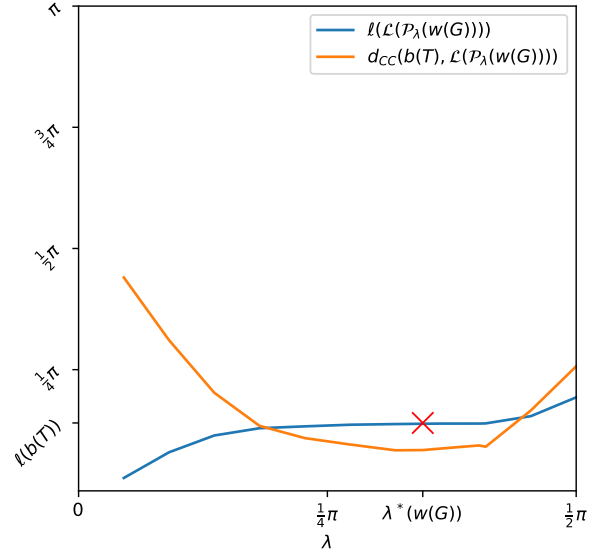

 (a) Validating Observations 1 and 2 for  $\mathbf{x} = \mathbf{e}(G)$ .

 (b) Evaluating the performance of  $\mathcal{L}(\mathbf{q}^*(\mathbf{e}(G)))$ 

 (c) Validating Observations 1 and 2 for  $\mathbf{x} = \mathbf{w}(G)$ .

 (d) Evaluating the performance of  $\mathcal{L}(\mathbf{q}^*(\mathbf{w}(G)))$ 

Figure 3: For a Planted Partition Model with  $n = 400$  vertices, partitioned into 20 equally sized communities with an average intra-community degree of 6 and an average inter-community degree of 2, the detection methods  $\mathcal{L}(\mathbf{q}^*(\mathbf{x}))$  for  $\mathbf{x} \in \{\mathbf{e}(G), \mathbf{w}(G)\}$  are evaluated. The crosses in Figures 3a and 3c denote the intersection point that is claimed by Empirical Observation 1 while Empirical Observation 2 claims that there is only one such intersection point. Theorem 7 suggests that the blue lines should roughly intersect the crosses of Figures 3b and 3d.

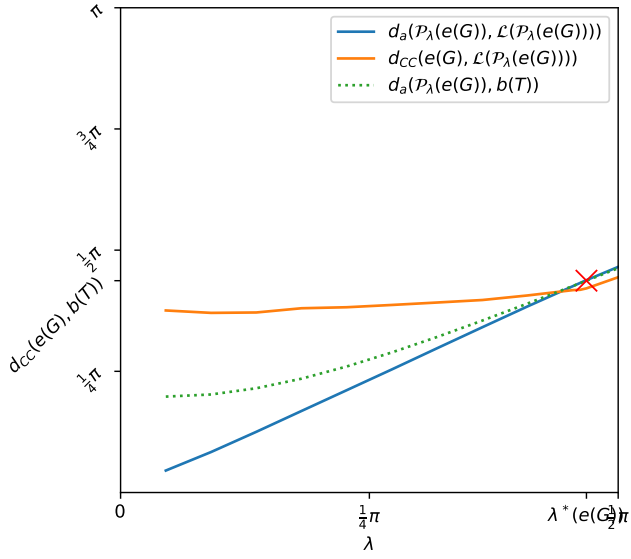
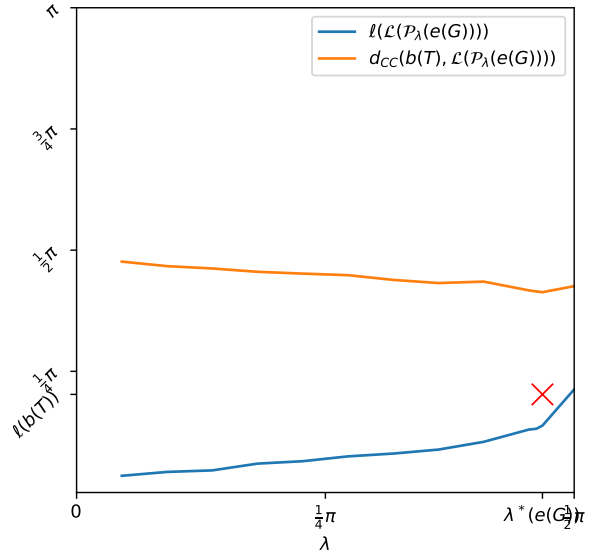
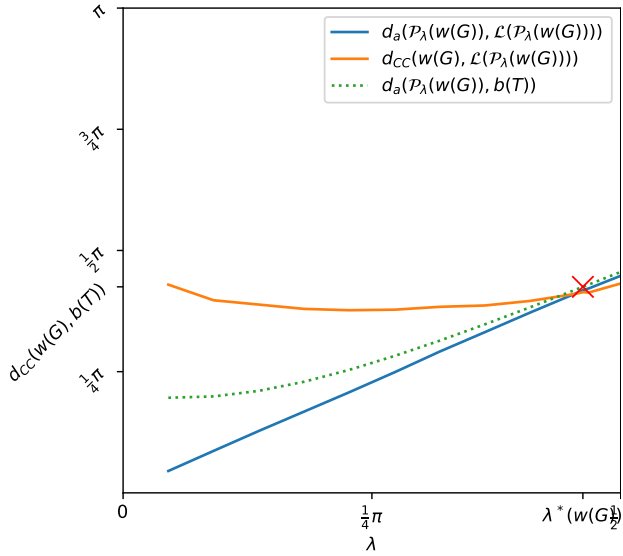
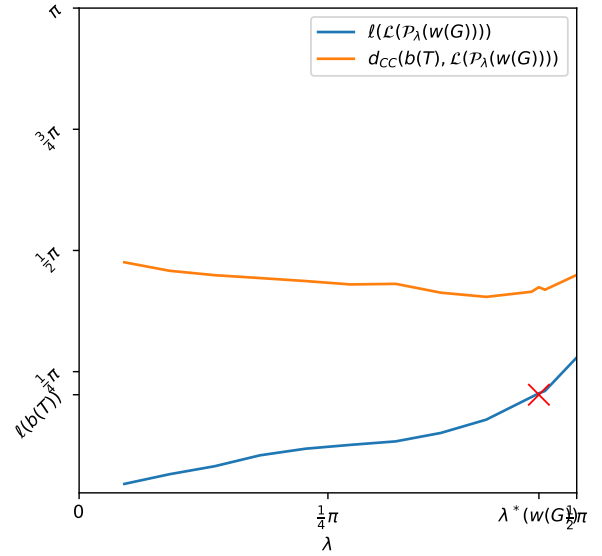
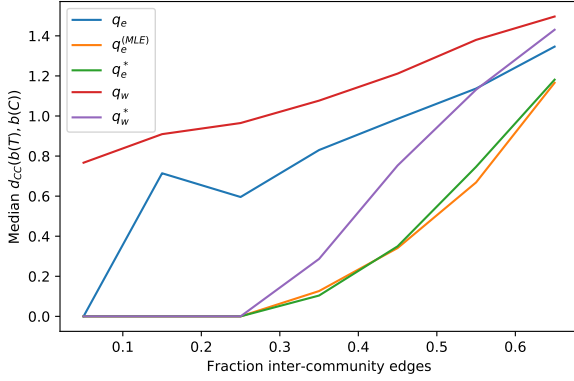
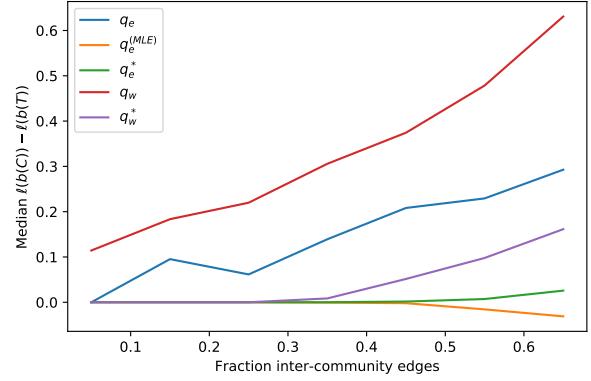

 (a) Validating Observations 1 and 2 for  $\mathbf{x} = \mathbf{e}(G)$ .

 (b) Evaluating the performance of  $\mathcal{L}(\mathbf{q}^*(\mathbf{e}(G)))$ 

 (c) Validating Observations 1 and 2 for  $\mathbf{x} = \mathbf{w}(G)$ .

 (d) Evaluating the performance of  $\mathcal{L}(\mathbf{q}^*(\mathbf{w}(G)))$ 

Figure 4: For a Planted Partition Model with  $n = 400$  vertices, partitioned into 10 equally sized communities with an average intra-community degree of 4 and an average inter-community degree of 4, the detection methods  $\mathcal{L}(\mathbf{q}^*(\mathbf{x}))$  for  $\mathbf{x} \in \{\mathbf{e}(G), \mathbf{w}(G)\}$  are evaluated. The crosses in Figures 4a and 4c denote the intersection point that is claimed by Empirical Observation 1 while Empirical Observation 2 claims that there is only one such intersection point. Theorem 7 suggests that the blue lines should roughly intersect the crosses of Figures 4b and 4d.

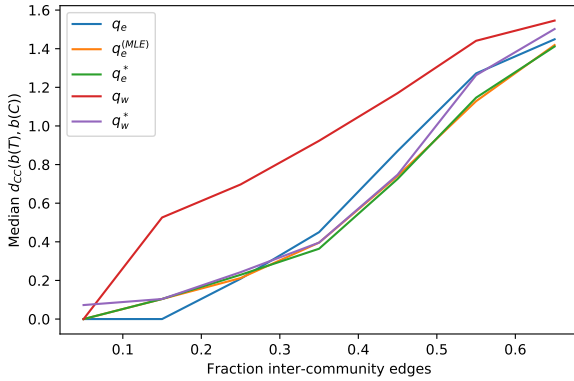


(a) Performance comparison

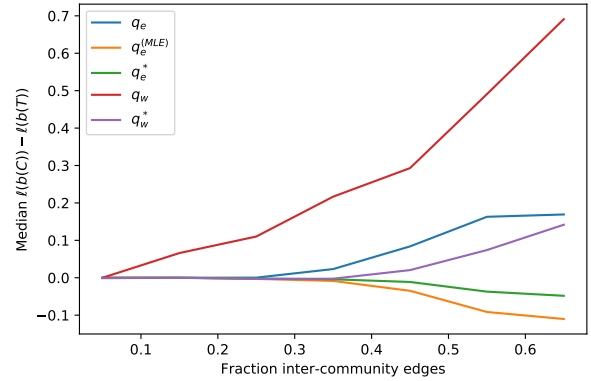


(b) Candidate latitudes comparison

Figure 5: For a Planted Partition Model with  $n = 400$ , partitioned into 40 equally sized communities with an average degree of 8, we vary the fraction of inter-community edges and plot the performance. Figure 5a shows the performance in terms of the correlation distance between candidate and ground truth clusterings, while Figure 5b shows the difference between the latitudes of the candidate and ground truth clusterings.

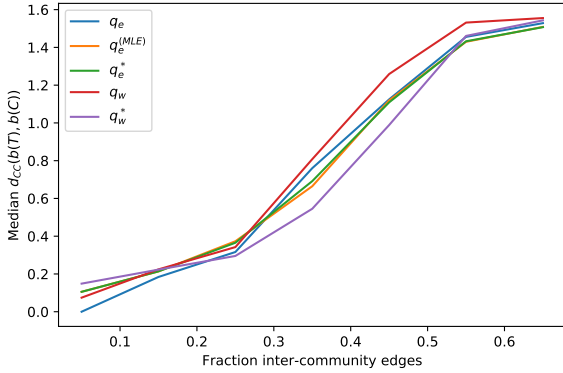


(a) Performance comparison

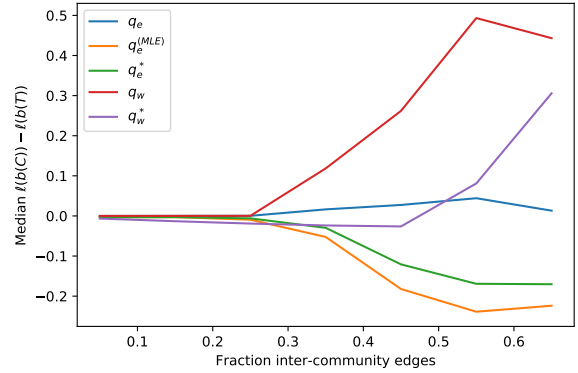


(b) Candidate latitudes comparison

Figure 6: For a Planted Partition Model with  $n = 400$ , partitioned into 20 equally sized communities with an average degree of 8, we vary the fraction of inter-community edges and plot the performance. Figure 6a shows the performance in terms of the correlation distance between candidate and ground truth clusterings, while Figure 6b shows the difference between the latitudes of the candidate and ground truth clusterings.

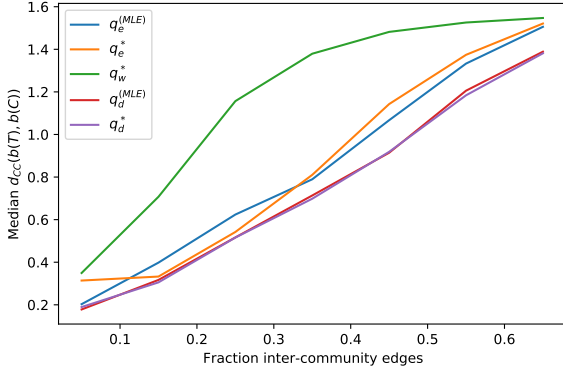


(a) Performance comparison

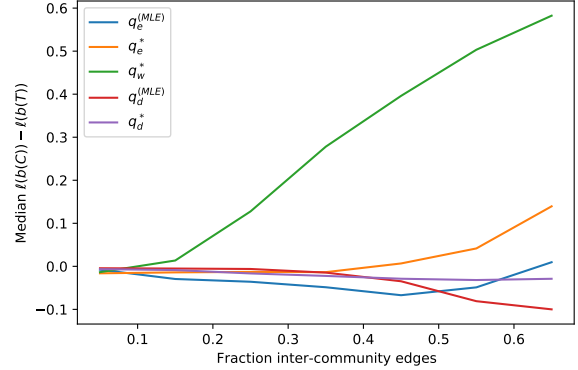


(b) Candidate latitudes comparison

Figure 7: For a Planted Partition Model with  $n = 400$ , partitioned into 10 equally sized communities with an average degree of 8, we vary the fraction of inter-community edges and plot the performance. Figure 7a shows the performance in terms of the correlation distance between candidate and ground truth clusterings, while Figure 7b shows the difference between the latitudes of the candidate and ground truth clusterings.



(a) Performance comparison



(b) Candidate latitudes comparison

Figure 8: For a Degree-Corrected Stochastic Block Model with  $n = 400$ , partitioned into 20 equally sized communities with an average degree of 8 and with power-law exponent 2.5, we vary the fraction of inter-community edges and plot the performance. Figure 8a shows the performance in terms of the correlation distance between candidate and ground truth clusterings, while Figure 8b shows the difference between the latitudes of the candidate and ground truth clusterings.

## 8. Discussion

In this work, we described a hyperspherical geometry on clusterings and showed how this geometry is related to validation measures such as the correlation distance. We then extended this geometry to include vectors that do not necessarily correspond to clusterings and proved that modularity maximization is equivalent to minimizing the distance to some modularity vector over the set of clustering vectors. This insight allowed us to describe a wide class of community detection methods containing all modularity-based methods, as well as other methods, in terms of this geometry. In the remainder of the paper, we explored this class of methods: we introduced a new community detection method based on the number of common neighbors that does not correspond to any modularity-based method and we developed a general method to ‘tune’ an input vector  $\mathbf{x}$  to obtain a suitable query vector.

This work opens up many avenues for future research. In the remainder of this section, we discuss the ones that are most promising in our opinion.

**Analysis and evaluation of the iterative algorithm.** Section 6.5 describes how Empirical Observation 2 may be utilized to develop an iterative variant of our geometric algorithm that has the advantage that it does not require any knowledge of the ground truth clustering. However, the analysis of this method comes with additional challenges, which is why we leave it for future research.

**Selection of input vector.** While the method described in Section 6.2 tells us how to choose a suitable query vector  $\mathbf{q}^*$  on the meridian of the input vector  $\mathbf{x}$ , it is not entirely clear how a suitable input vector should be chosen. In Section 6.4 it has been discussed that  $\mathbf{x}$  should contain information about the ground truth  $\mathbf{b}(T)$  and that the correlation distance  $d_{CC}(\mathbf{x}, \mathbf{b}(T))$  seems to be a reasonable measure to quantify this. To this end,  $\mathbf{x}$  could be obtained as some (linear) combination of other vectors such as  $\mathbf{e}(G)$ ,  $\mathbf{w}(G)$  and others in order to minimize  $d_{CC}(\mathbf{x}, \mathbf{b}(T))$ . However, obviously such an optimization would require even more knowledge of the ground truth  $\mathbf{b}(T)$ .

**Projections in other geometries.** We proved that maximizing modularity is equivalent to minimizing the angular distance to a query vector. This begs the question whether minimizing other distances would also give good community detection methods. In particular, it would be interesting to investigate minimizing the correlation distance instead of the angular distance, as this distance would allow one to bound the correlation distance between candidate and ground truth clusterings by their correlation distances to the query vector. Furthermore, since the correlation distance is a distance between meridians (as proven by Theorem 1), there would be no need to tune the latitude of the query vector.

**Improved modularity optimization algorithms.** Finally, as we have proven that the Louvain algorithm is essentially an approximate nearest-neighbor algorithm, it would be interesting to see whether existing approximate nearest-neighbor algorithms outperform the Louvain algorithm in terms of the obtained modularity value or in terms of running time. At any rate, it may be interesting to investigate whether the geometry may be utilized to improve upon Louvain or other modularity-optimizing algorithms.

**Acknowledgements.** The work of MG and RvdH is supported in part by the Netherlands Organisation for Scientific Research (NWO) through the Gravitation NETWORKS grant no. 024.002.003.

## References

- Ahmed N Albatineh, Magdalena Niewiadomska-Bugaj, and Daniel Mihalco. On similarity indices and correction for chance agreement. *Journal of Classification*, 23(2):301–313, 2006.
- Alex Arenas, Alberto Fernandez, and Sergio Gomez. Analysis of the structure of complex networks at different resolution levels. *New journal of physics*, 10(5):053039, 2008.
- Vincent D Blondel, Jean-Loup Guillaume, Renaud Lambiotte, and Etienne Lefebvre. Fast unfolding of communities in large networks. *Journal of statistical mechanics: theory and experiment*, 2008 (10):P10008, 2008.
- Ulrik Brandes, Daniel Delling, Marco Gaertler, Robert Gorke, Martin Hoefer, Zoran Nikoloski, and Dorothea Wagner. On modularity clustering. *IEEE transactions on knowledge and data engineering*, 20(2):172–188, 2007.
- Joseph D Donnay. *Spherical trigonometry*. Read Books Ltd, 2011.
- Maurizio Filippone, Francesco Camastra, Francesco Masulli, and Stefano Rovetta. A survey of kernel and spectral methods for clustering. *Pattern recognition*, 41(1):176–190, 2008.
- Santo Fortunato. Community detection in graphs. *Physics reports*, 486(3-5):75–174, 2010.
- Santo Fortunato and Marc Barthélemy. Resolution limit in community detection. *Proceedings of the National Academy of Sciences*, 104(1):36–41, 2007. ISSN 0027-8424. doi: 10.1073/pnas.0605965104. URL <https://www.pnas.org/content/104/1/36>.
- Martijn Gösgens, Liudmila Prokhorenkova, and Alexey Tikhonov. Systematic analysis of cluster similarity indices: Towards bias-free cluster validation, 2019.
- Lawrence Hubert. Nominal scale response agreement as a generalized correlation. *British Journal of Mathematical and Statistical Psychology*, 30(1):98–103, 1977. doi: 10.1111/j.2044-8317.1977.tb00728.x. URL <https://onlinelibrary.wiley.com/doi/pdf/10.1111/j.2044-8317.1977.tb00728.x>.
- Paul Jaccard. The distribution of the flora in the alpine zone. 1. *New phytologist*, 11(2):37–50, 1912.
- Jussi M Kumpula, Jari Saramäki, Kimmo Kaski, and János Kertész. Limited resolution in complex network community detection with potts model approach. *The European Physical Journal B*, 56(1):41–45, 2007.
- Andrea Lancichinetti and Santo Fortunato. Limits of modularity maximization in community detection. *Physical review E*, 84(6):066122, 2011.
- Yang Lei, James C. Bezdek, Simone Romano, Nguyen Xuan Vinh, Jeffrey Chan, and James Bailey. Ground truth bias in external cluster validity indices. *Pattern Recognition*, 65:58 – 70, 2017. ISSN 0031-3203. doi: <https://doi.org/10.1016/j.patcog.2016.12.003>. URL <http://www.sciencedirect.com/science/article/pii/S0031320316303910>.
- Mark EJ Newman. Equivalence between modularity optimization and maximum likelihood methods for community detection. *Physical Review E*, 94(5):052315, 2016.
- Mark EJ Newman and Michelle Girvan. Finding and evaluating community structure in networks. *Physical review E*, 69(2):026113, 2004.

- Liudmila Prokhorenkova. Using synthetic networks for parameter tuning in community detection. In *International Workshop on Algorithms and Models for the Web-Graph*, pages 1–15. Springer, 2019.
- Liudmila Prokhorenkova and Alexey Tikhonov. Community detection through likelihood optimization: in search of a sound model. In *The World Wide Web Conference*, pages 1498–1508, 2019.
- William M Rand. Objective criteria for the evaluation of clustering methods. *Journal of the American Statistical association*, 66(336):846–850, 1971.
- Jörg Reichardt and Stefan Bornholdt. Statistical mechanics of community detection. *Physical review E*, 74(1):016110, 2006.
- Simone Romano, Nguyen Xuan Vinh, James Bailey, and Karin Verspoor. Adjusting for chance clustering comparison measures. *The Journal of Machine Learning Research*, 17(1):4635–4666, 2016.
- Isaac Todhunter. *Spherical trigonometry, for the use of colleges and schools: with numerous examples*. Macmillan, 1863.
- Vincent A Traag, Paul Van Dooren, and Yurii Nesterov. Narrow scope for resolution-limit-free community detection. *Physical Review E*, 84(1):016114, 2011.
- Vincent A Traag, Ludo Waltman, and Nees Jan van Eck. From louvain to leiden: guaranteeing well-connected communities. *Scientific reports*, 9(1):1–12, 2019.
- Nguyen Xuan Vinh, Julien Epps, and James Bailey. Information theoretic measures for clusterings comparison: is a correction for chance necessary? In *Proceedings of the 26th annual international conference on machine learning*, pages 1073–1080, 2009.
- Nguyen Xuan Vinh, Julien Epps, and James Bailey. Information theoretic measures for clusterings comparison: Variants, properties, normalization and correction for chance. *The Journal of Machine Learning Research*, 11:2837–2854, 2010.
- Rui Xu and Donald Wunsch. Survey of clustering algorithms. *IEEE Transactions on neural networks*, 16(3):645–678, 2005.

## Appendix A. Additional proofs

**Lemma 8** *The latitude of the modularity vector for the Erdős-Rényi null model is given by*

$$\tan \ell(\mathbf{q}_M(G; \text{ER}, \gamma)) = \frac{\sqrt{\frac{N-m_G}{m_G}}}{\gamma - 1}.$$

**Proof** Note that we have  $\mathbf{p}(G; \text{ER}) = \frac{m_G}{N} \mathbf{1}$  so that  $\|\mathbf{p}(G; \text{ER})\|^2 = \frac{m_G^2}{N}$  and

$$\langle \mathbf{p}(G; \text{ER}), \mathbf{e}(G) \rangle = 2 \frac{m_G^2}{N} - m_G.$$

We substitute these into (17) and rewrite the result to

$$\begin{aligned}\cos \ell(\mathbf{q}_M(G; \text{ER}, \gamma)) &= \frac{(\gamma - 1)m_G}{\sqrt{N} \cdot \sqrt{(1 - \gamma)m_G + \gamma^2 \frac{m_G^2}{N} - \gamma(2 \frac{m_G^2}{N} - m_G)}} \\ &= \frac{(\gamma - 1) \frac{m_G}{N}}{\sqrt{\left((\gamma - 1) \frac{m_G}{N}\right)^2 + \frac{m_G(N - m_G)}{N^2}}}.\end{aligned}$$

Therefore, the tangent is given by

$$\tan \ell(\mathbf{q}_M(G; \text{ER}, \gamma)) = \frac{\sqrt{1 - \cos^2 \ell(\mathbf{q}_M(G; \text{ER}, \gamma))}}{\cos \ell(\mathbf{q}_M(G; \text{ER}, \gamma))} = \frac{\sqrt{\frac{m_G(N - m_G)}{N^2}}}{(\gamma - 1) \frac{m_G}{N}} = \sqrt{\frac{N - m_G}{m_G}},$$

as required. ■

**Lemma 9** *The Louvain algorithm is a projection. That is,  $\mathcal{L}(\mathcal{L}(\mathbf{q})) = \mathcal{L}(\mathbf{q})$  for any query vector  $\mathbf{q} \in \mathbb{R}^N$ .*

**Proof** We equivalently prove that for any clustering  $C$ , Louvain maps the query vector  $\mathbf{q} = \mathbf{b}(C)$  to itself, i.e.  $\mathcal{L}(\mathbf{b}(C)) = \mathbf{b}(C)$ . Recall that the Louvain algorithm is initialized at the fine pole, i.e. the clustering consisting of  $n$  singleton clusters. Then, it iterates through all vertices and relabels each vertex greedily. That is, a vertex is assigned to the cluster that results in the largest decrease in the angular distance to the query vector, or equivalently, the largest increase of  $\langle \mathbf{b}(C'), \mathbf{b}(C) \rangle$ , where  $C'$  is the new candidate clustering after relabeling.

Let us consider one cluster  $c \in C$ . The first time that the iteration of Louvain encounters a vertex  $i \in c$ , all of its cluster-members will be assigned to singleton clusters so that  $i$  will be relabeled to the cluster of any of its cluster-members  $j \in c \setminus \{i\}$  arbitrarily. Then, the next time a vertex  $k \in c \setminus \{i, j\}$  is encountered in the iteration, the greedy choice will be to relabel  $k$  the cluster  $\{i, j\}$ , as it results in a larger increase than relabeling  $k$  to any of the singleton clusters of  $c \setminus \{i, j, k\}$ . Similarly, all other vertices of  $c$  will be relabeled to this cluster so that the resulting Louvain candidate will contain the cluster  $c$ . In the same way, all other clusters  $c' \in C$  will be obtained so that indeed  $\mathcal{L}(\mathbf{b}(C)) = \mathbf{b}(C)$ . ■